

Airborne Wind Profiling Portable Radar (AWiPPR)



Marshall Bradley, Mark Henderson and Michael Vollmuth
LogLinear Group

Quinn Smith
QinetiQ Inc.

November 2021



Introduction

In 2015 LogLinear completed development of the Wind Profiling Portable Radar (WiPPR) system and began development of an airborne version. We refer to the airborne version of WiPPR as AWiPPR. Because of numerous complications associated with the motion of the aircraft, the AWiPPR problem is more complicated than WiPPR. However the two systems share similar electronics and as a first cut, AWiPPR is just WiPPR turned upside down and mounted on an aircraft of opportunity.

This document provides a description of the physics supporting the AWiPPR system and contains many examples of AWiPPR performance.

AWiPPR Terminology

Like all frequency modulated continuous wave (FMCW) radars, the AWiPPR system measures six fundamental quantities. Three of these are scalar and one is a vector. Specifically they are the slant range to a target R , the echo power S of the target reflection, the Doppler velocity V of the echo and an estimate of the vector direction $\boldsymbol{\eta}$ in which the radar beam was pointing at the time of the measurement. The determination of this last quantity requires supporting navigational data. The navigational data measured by AWiPPR includes the vector velocity of the aircraft together with roll, pitch and yaw angles of the airframe with respect to level flight. In terms of an inertial xyz Cartesian coordinate system where x is west to east displacement, y is south to north displacement and z is altitude above ground level, the beam pointing direction can be written in terms of direction cosines, i.e. $\boldsymbol{\eta} = (\cos X, \cos Y, \cos Z)$. The relationship between slant range of the echo and the altitude of the echo above ground level for an ground based radar is $z = R \cos Z$. For an airborne radar at height h above ground level $z = h - R \cos Z$. The relationship between measured Doppler velocity of the echo, the vector velocity of the wind and the vector velocity of the aircraft is

$$V_{measured} = (\mathbf{v}_{radar} - \mathbf{v}_{wind}) \cdot \boldsymbol{\eta}$$

where \mathbf{v}_{radar} is the radar velocity (same thing as aircraft velocity) and \mathbf{v}_{wind} is the wind velocity vector. One of the first things that takes place in the AWiPPR signal processing

chain is to correct all Doppler velocities for the velocity of the radar. After this is done the Doppler-wind velocity relationship becomes

$$V_{measured} = - \mathbf{v}_{wind} \cdot \boldsymbol{\eta} = - (v_x \cos X, v_y \cos Y, v_z \cos Z)$$

The unknowns in this equation are the wind velocity components (v_x, v_y, v_z) . The knowns are the motion corrected Doppler velocity $V_{measured}$ and the direction cosines of the radar beam pointing direction $(\cos X, \cos Y, \cos Z)$. Thus we have one equation and three unknowns. This tells us that it is not possible to determine wind velocity at an altitude from a single Doppler velocity measurement at that altitude.

In order to infer wind velocity from the Doppler measurements, multiple Doppler velocity measurements are required. WiPPR achieves this diversity by rotating the radar beam mechanically. AWiPPR achieves this directional diversity by turning the aircraft and collecting data as the radar turns (see figure 1 next page). The necessary directional diversity could also be obtained by physically turning the radar antennas as marine radars do or by using an electronically steerable transmit antenna. At the initial stage of development of the AWiPPR system it made more economic sense to change the direction of the aircraft.

AWiPPR Range Velocity Matrix Formation

The fundamental AWiPPR data structures are range-velocity matrices (RVMs) and data cubes. A data cube is a stack of 200 RVMs spanning a time interval of 10 sec. Each AWiPPR frequency modulated pulse is 190 microsecond in length with a sweep width of 48 MHz. An RVM is formed by placing raw AWiPPR echo data into a data stack (also called matrix). The individual pulses are each $NFFT=4096$ samples long and are located in the vertical columns of this stack. This is repeated $Q=256$ times to form the entire data stack. The vertical axis in the matrix is known as fast time and the horizontal axis is slow time. The time sampling interval in fast time is $T_m/NFFT$ where T_m is the radar pulse length. Sampling in slow time is at steps of T_m . Referring to figure 2. **a)** An FFT is applied to the vertical columns of the data stack in order to resolve targets in range. This step resolves the beat frequencies in the down-mixed radar echoes that arise from their round-trip time delay. In particular this step resolves the ground echo into a bright band located at the slant range to the ground.

To resolve targets in Doppler velocity, FFTs are performed horizontally for each row in the data-matrix shown in step a). The processing gain in moving from raw data to b) is $10\log(NFFT \times Q)$. The data-matrix b) is referred to as the range-velocity matrix. The dimensions of the range-velocity matrix are $NFFT/2=2048$ rows by $Q=256$ columns. Hanning windows are applied in both stages of FFTs in order to reduce spectral leakage. The next step in the AWiPPR processing chain is formation of a data cube through the association of time sequential RVMs. An AWiPPR data cube has three axes: slant range R , Doppler velocity V and slow time T . Echoes are detected in VR space by marginalizing (averaging with the appropriate time scale) across the T dimension in the radar data cube. Examples of this will be shown in the material that follows.

Figure 1. AWiPPR geometry.

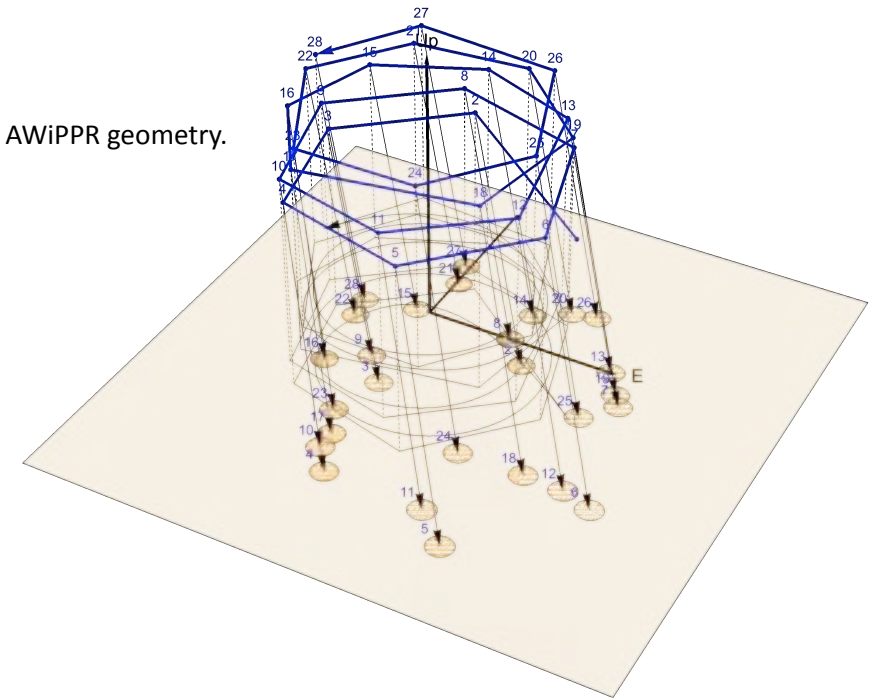
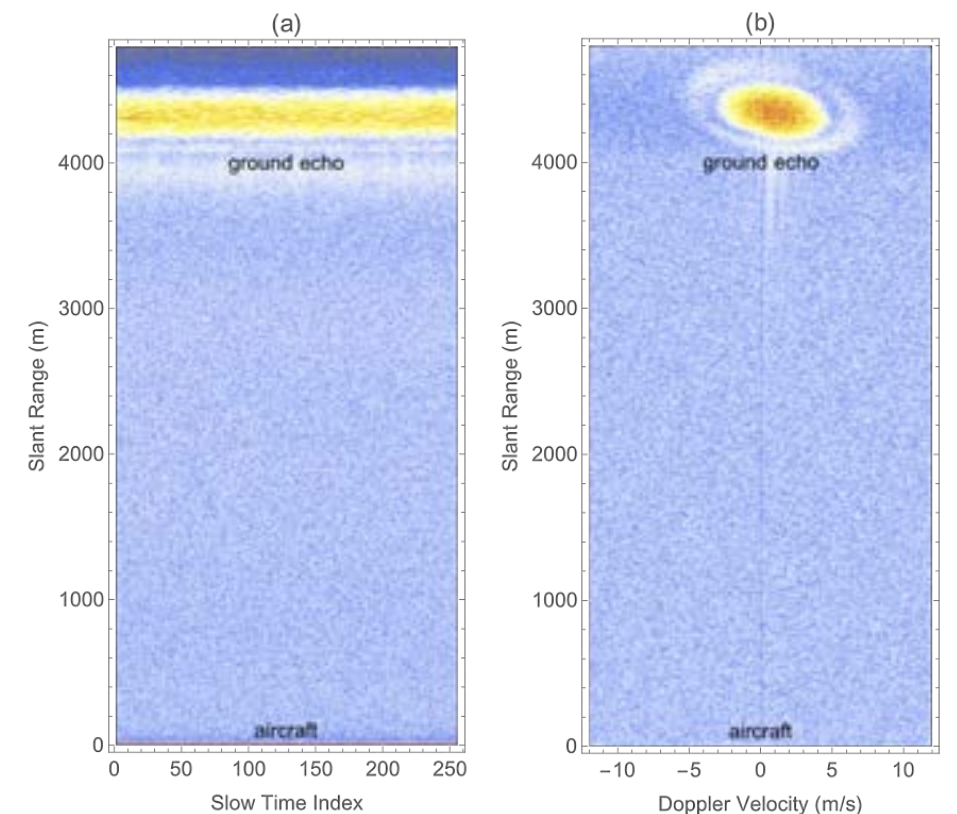
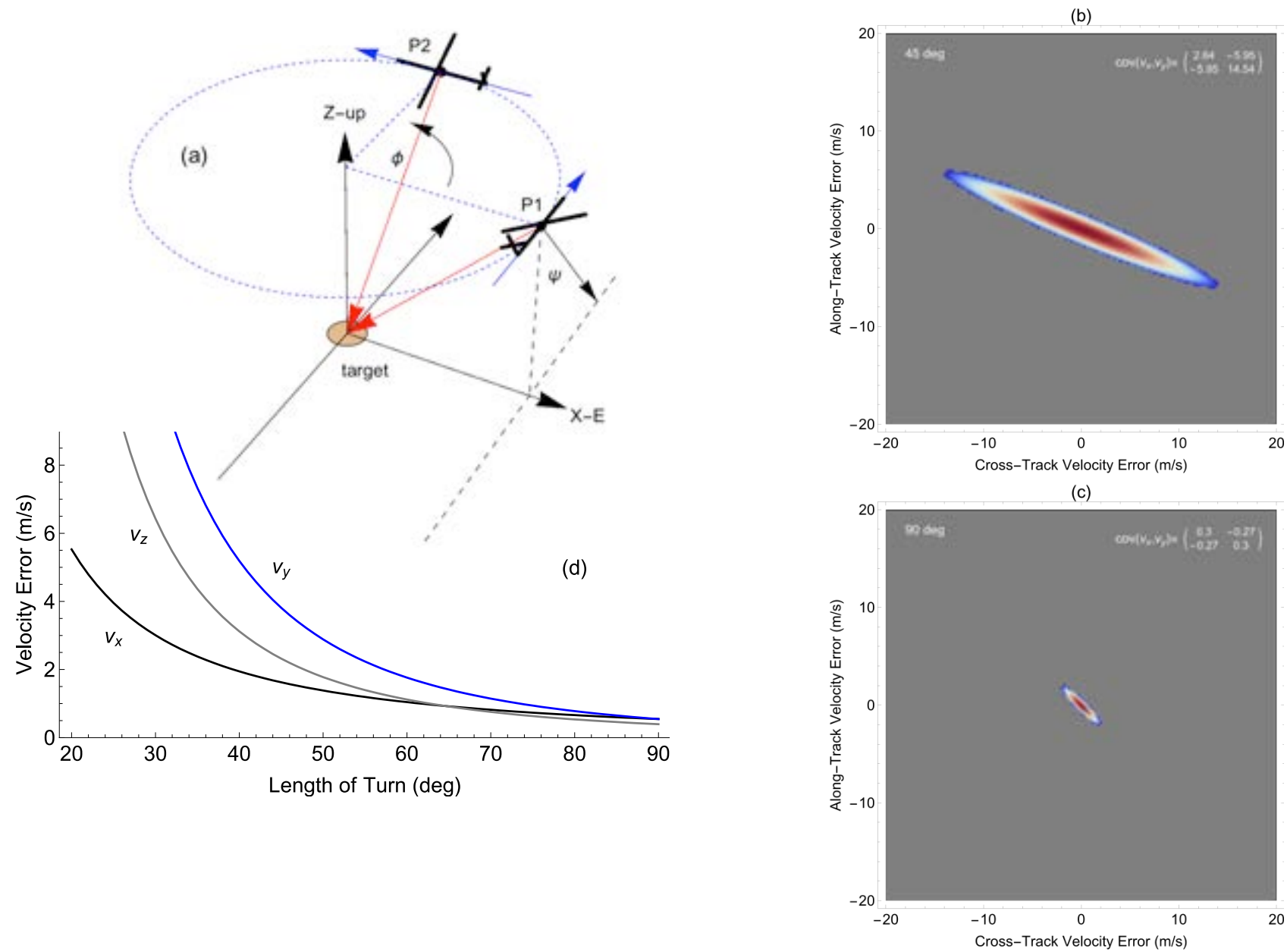


Figure 2. RVM formation.



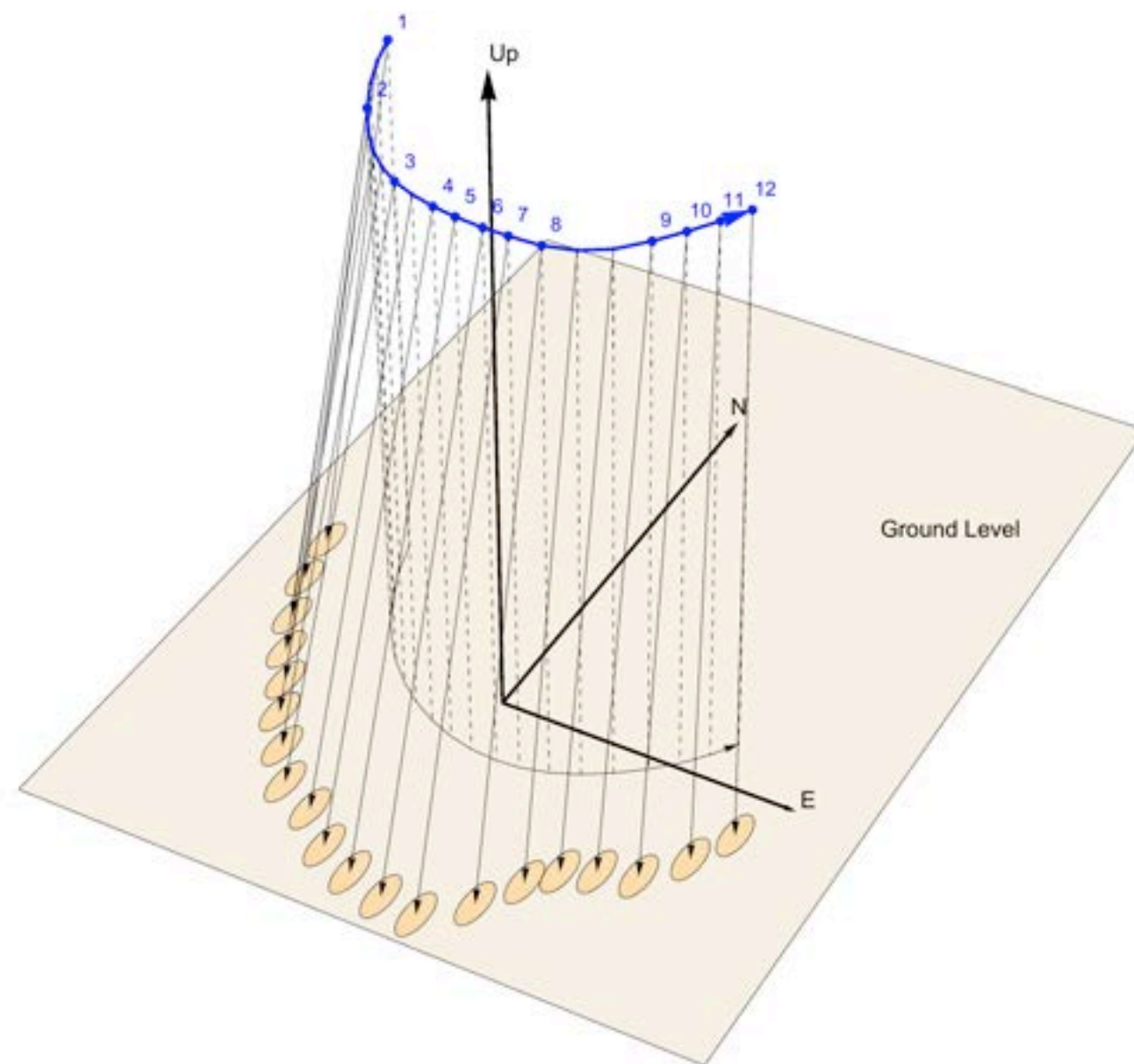


Early concept for an airborne WiPPR for use in support of C130 gunship operations.

An early idea for AWiPPR support to C130 gunship operations employing a single beam radar which achieves beam diversity by turning is shown above. (a) C130 flight path during weapon's fire and the instantaneous direction of the AWiPPR radar beam. (b) AWiPPR velocity error surface for 45 deg turn. (c) AWiPPR velocity error surface for 90 deg turn. (d) Cross-track, along-track and up-down velocity errors for a range of C130 turn angles.

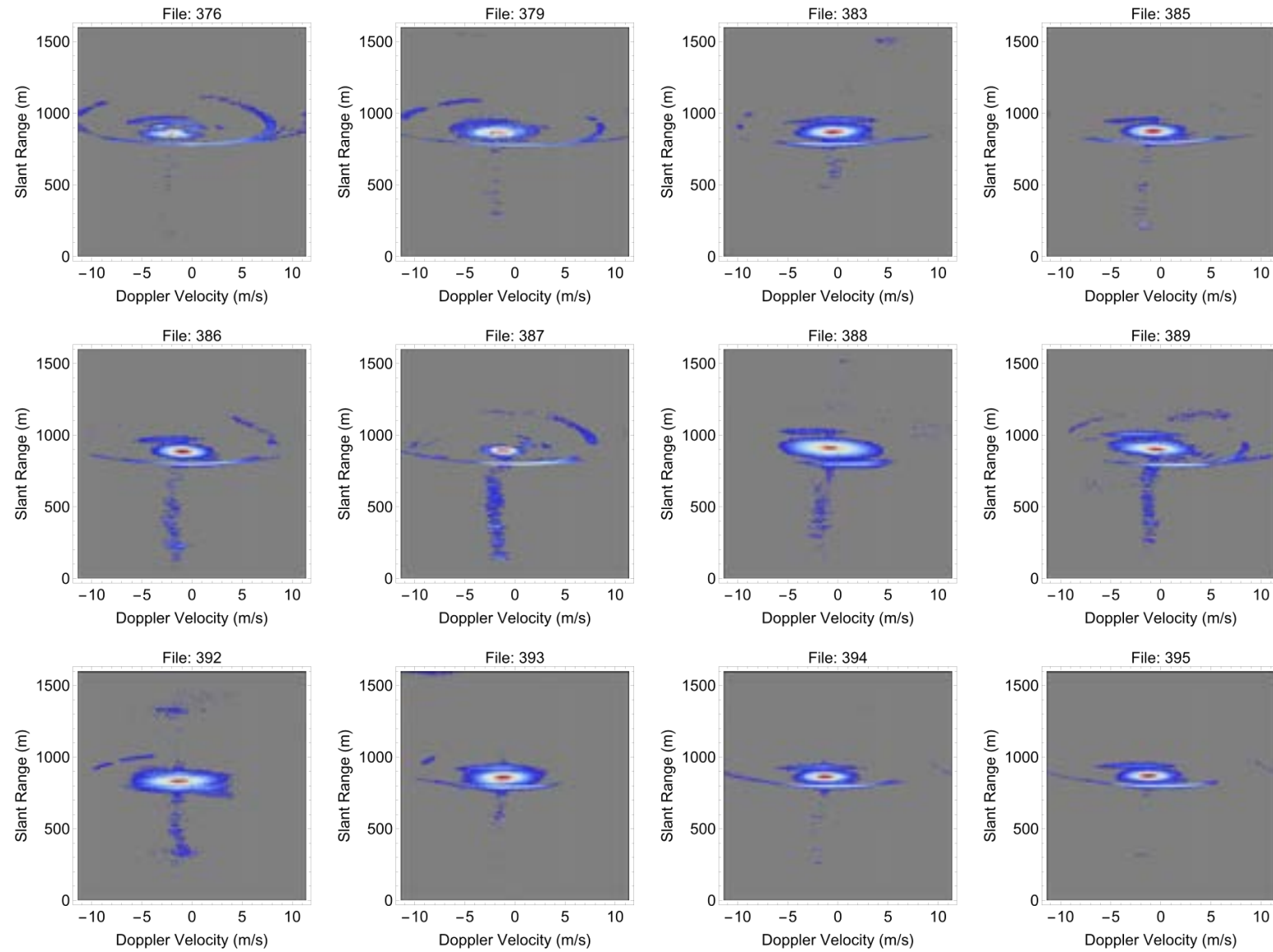
Initial Success

On 6 May 2016 a prototype version of the AWiPPR system was operated over Bay St. Louis, MS. We were able to detect echoes from clear air scatter (convective turbulence) when the system was over the bay but not over land. This section documents some of our results from those measurements. These measurements were instrumental in setting the entire program on the path to success. In particular they document the negative effects of saturation in the radar receiver on system performance and set the stage for a change in operating tactics.



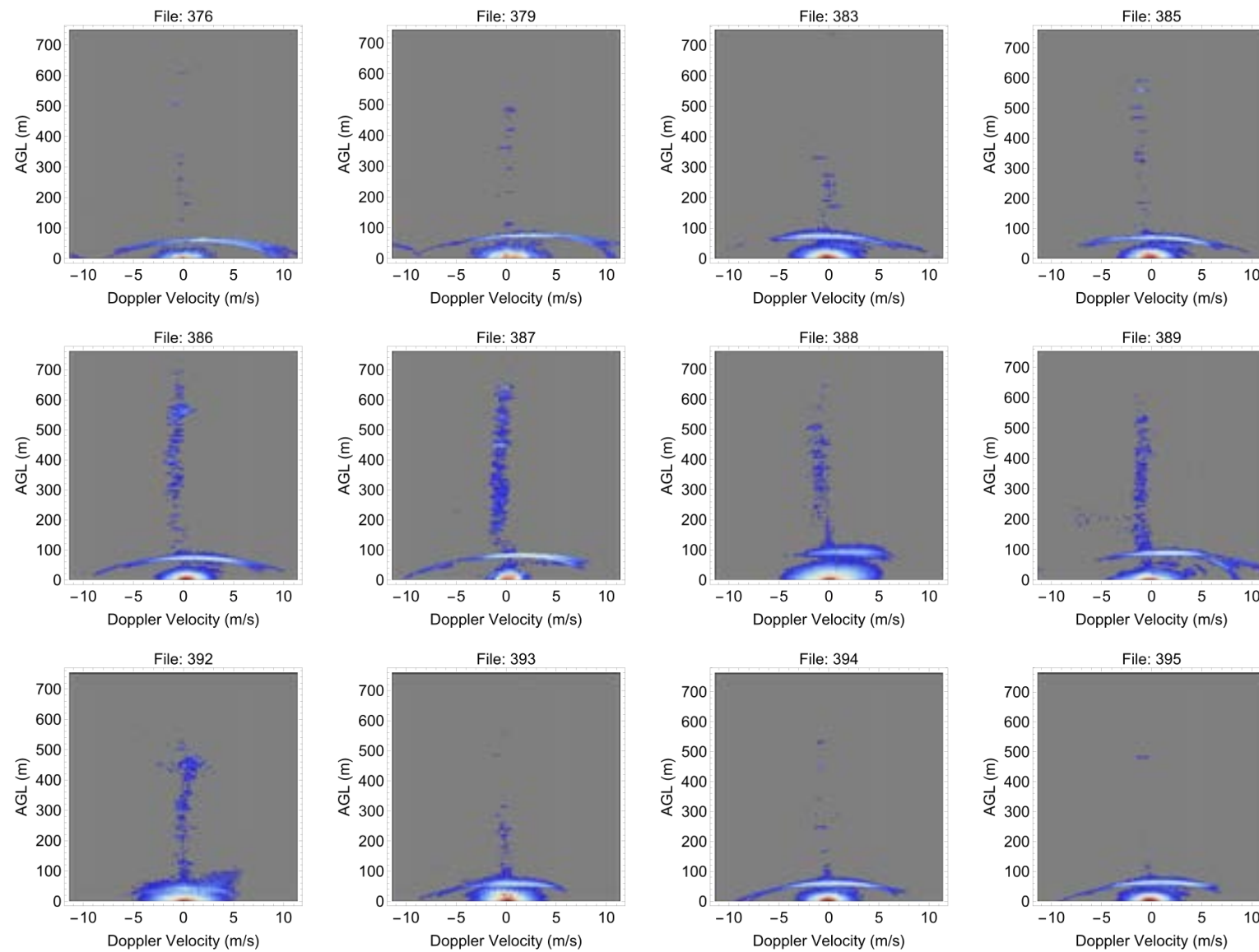
AWiPPR turn maneuver from 6 May 2016 when AWiPPR made first successful wind velocity measurement.

A pictorial representation of the turning maneuver used by AWiPPR on its initial flight on 6 May 2016 is shown above. The ellipses on the sea level reference plane in the figure indicate the regions where the dominant amount of surface scatter occurred. The dashed lines in the figure are the normals to the surface of the earth. During the turn shown in the figure, range velocity matrices were recorded. Twelve of the range velocity matrices were found to contain echoes from the winds in that portion of the convective boundary layer beneath the aircraft.



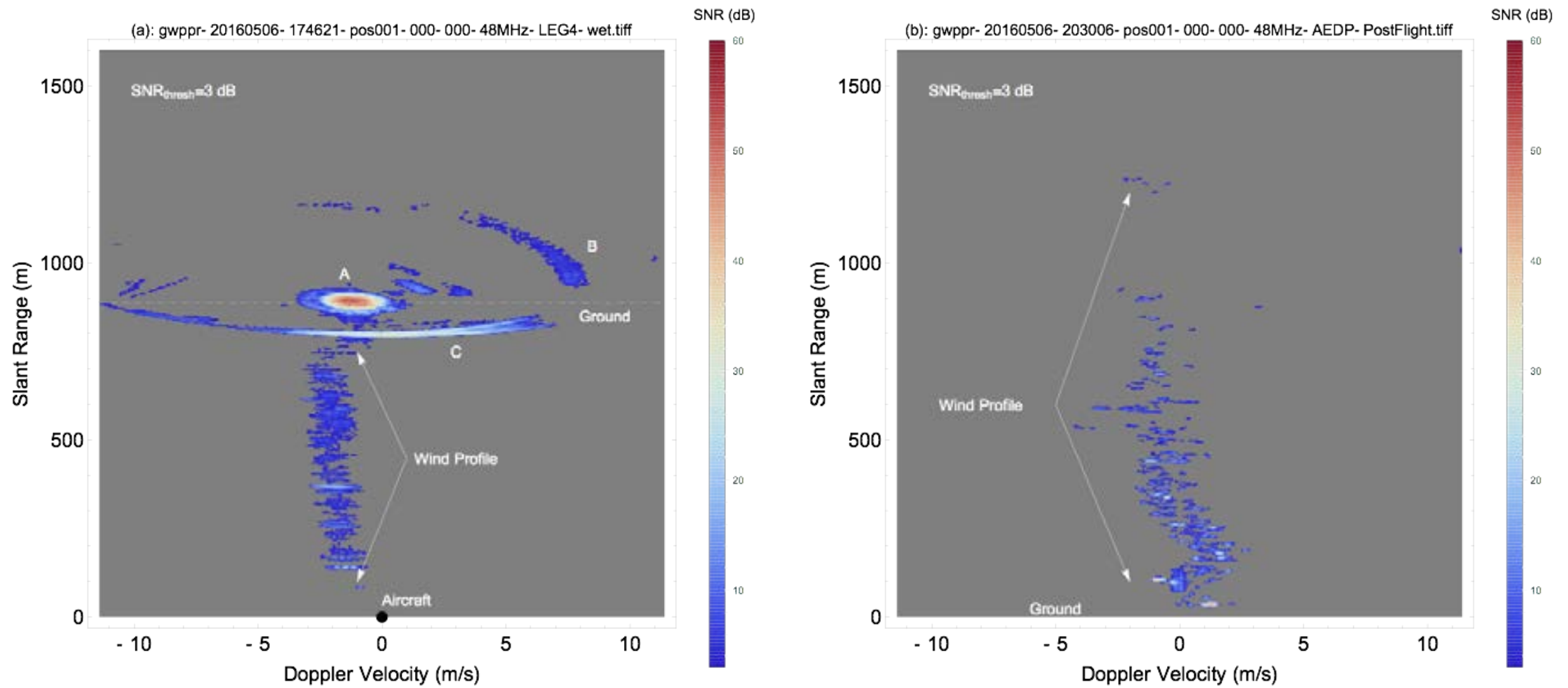
Part 1) RVM data from AWiPPR turn maneuver on 6 May 2016

The above show the range velocity matrices as measured. The strong ground bounce is located at a slant range slightly less than 1000 m. The plane is flying at an altitude of 800 m. Echos closest to the plane occur at the bottom of these figures.



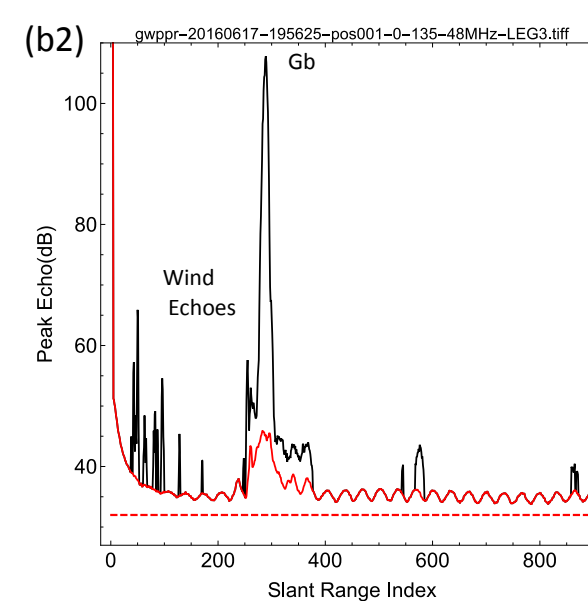
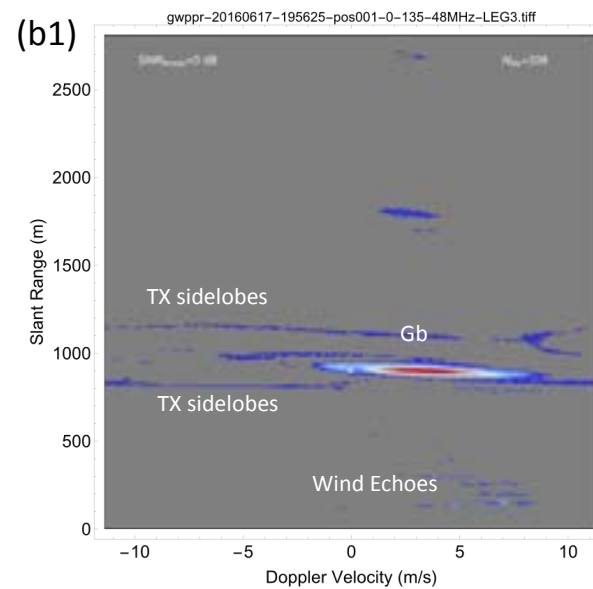
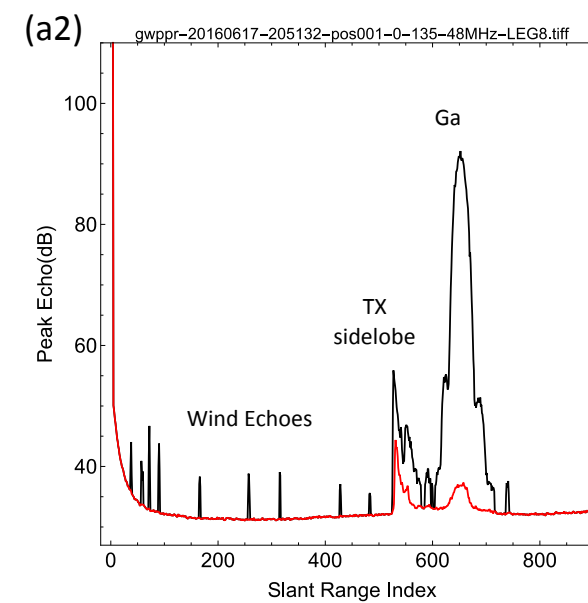
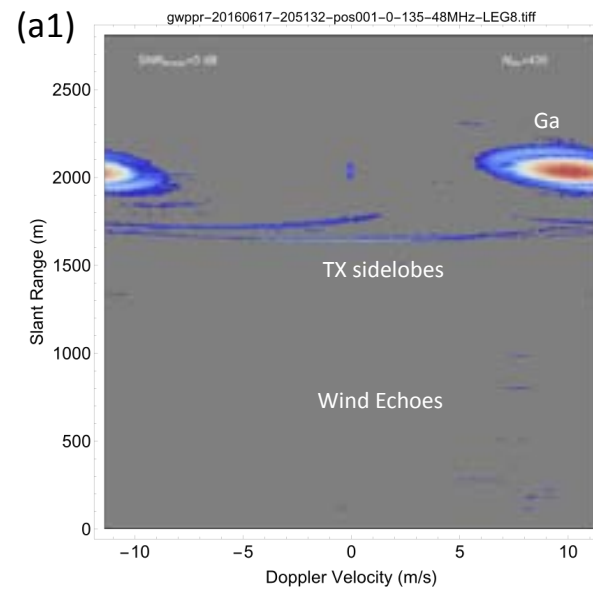
Part 2) RVM data from AWiPPR turn maneuver on 6 May 2016.

The above show the range velocity matrices with ground bounce brought to zero Doppler and the peak echo placed at zero range. The wind profile at different azimuthal angles shows up in most of these images. The key point here is that AWiPPR is measuring winds beneath the aircraft and above the surface of Bay Saint Louis.



Part 3) RVM data from AWiPPR turn maneuver on 6 May 2016.

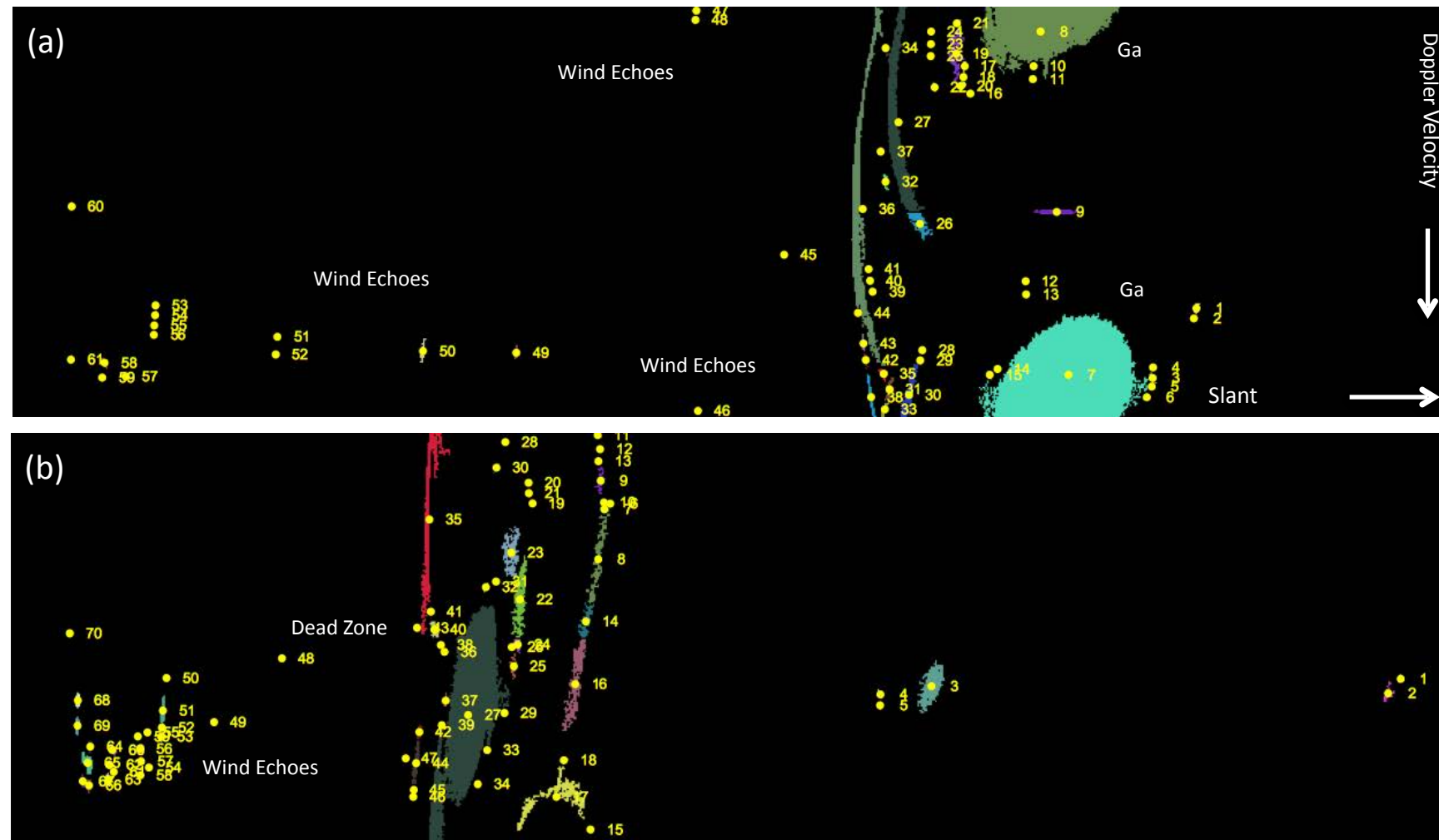
The above figures show measurement of the Doppler wind speed profile with the AWiPPR system operating in (a) downward-looking in-flight mode and (b) upward-looking ground-based mode. The aircraft is operating at an altitude of approximately 800 m in (a) over the waters of Bay St. Louis, MS.



Part 1) Effect of saturation from the ground echo on AWiPPR performance.

With reference to the above figures. (a) Radar performance is limited by the noise floor. (b) Radar performance is limited by saturation from the peak ground echo. In the range velocity matrices a1 and b1, the peak ground echo is denoted by Ga and Gb. Positions of wind echoes are denoted in the figures. Plots (a2) and (b2) are the slant range marginals of the RVMs (a1) and (a2). Peak marginal is indicated by the black lines and the median marginal is indicated by the red line. This latter quantity is referred to as the noise floor. In (a2) the noise floor is at

approximately 32 dB except near slant range index zero and ranges where there is a very large echo. The dashed red line in (b2) is a 32 dB reference. Notice how the noise floor in (b2) oscillates. This is an indication that the radar system has been saturated by a strong echo which in this case is the ground echo Gb. Saturation raises the effective level of the noise floor and makes it impossible to detect wind echoes that have insufficient SNR. With reference to (a1) and (b1), the aircraft is located at slant range zero.

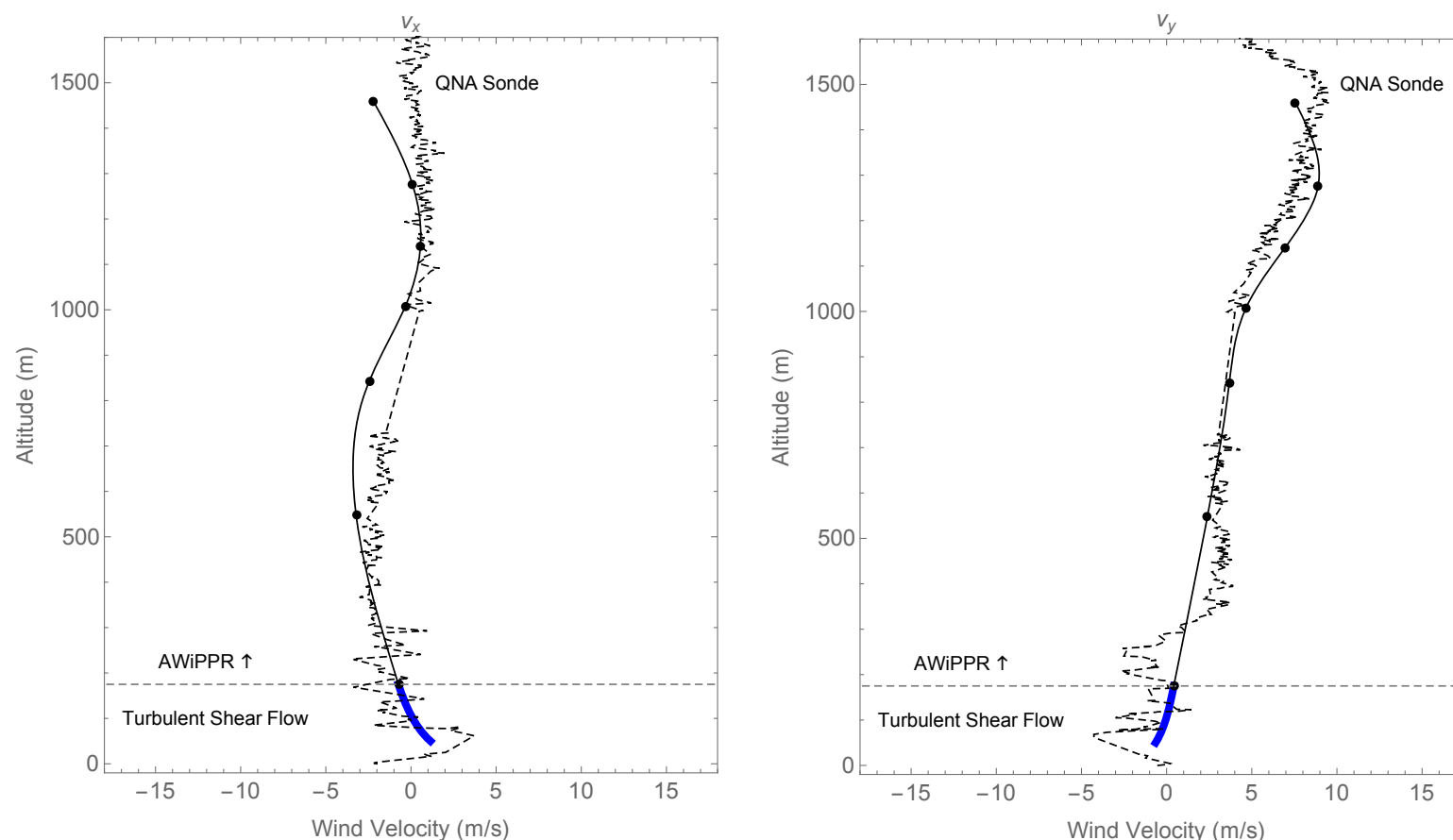


Part 2) Effect of saturation from the ground echo on AWiPPR performance.

In the above, color is used to visually separate connected morphological features with $\text{SNR} > 3$ dB. Features with fewer than 4 pixels have been dropped. The horizontal axis in the images is slant range and the vertical axis is Doppler velocity. In (a) morphological features 45-60 are wind echoes. Note how features 53-56 are closely spaced together. This represents a target crossing the radar beam that comes in and out of detection possibly due to sampling. Note how morphological feature 50 is extended in Doppler velocity. This is also a target

crossing the radar beam but the target has stayed continuously in view. Features 46-48 are similar but there is velocity wrapping. Features 7-8 are the main portion of the ground echo which has been split apart by Doppler velocity wrapping. In part (b) features 48-70 are wind echoes. In (b) there is a substantial dead zone between features 48 and the ground echo region. No wind echoes are detected here even though the radar is much closer to the ground than in part (a).

Achievement of AWiPPR Goals



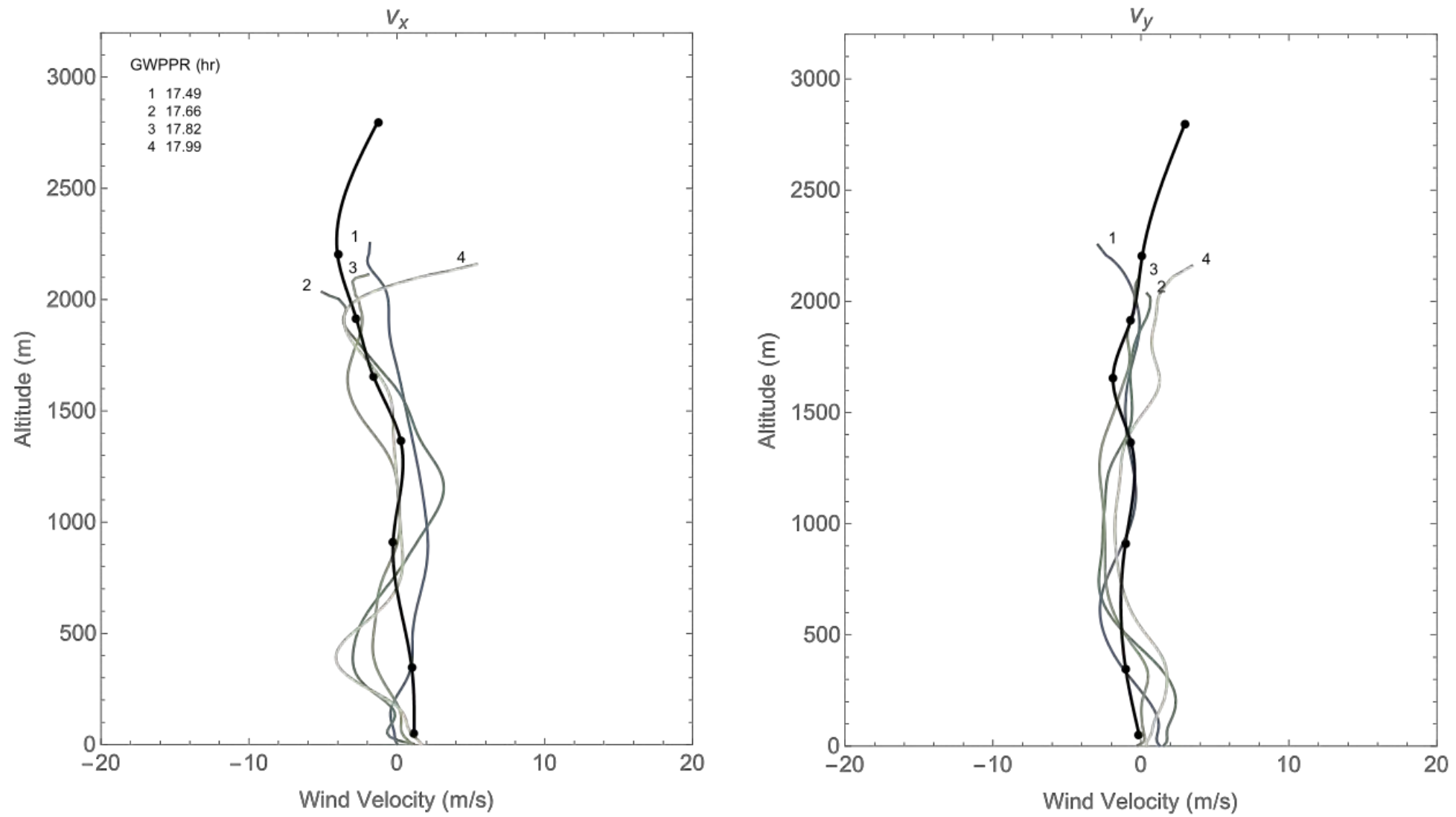
AWiPPR measurements from October 2016. Blue lines are an attempt to model winds in lower 200 m using a logarithmic turbulent shear flow model.

By October of 2016 we were operating AWiPPR at 1600 m above ground and obtaining wind profiles down to within 200 m of the ground. These profiles were found to be in good agreement with wind speed profiles measured by ground launched radio sondes. By August 2017 we had increased operating height to 3000 m. By program end in 2018 we

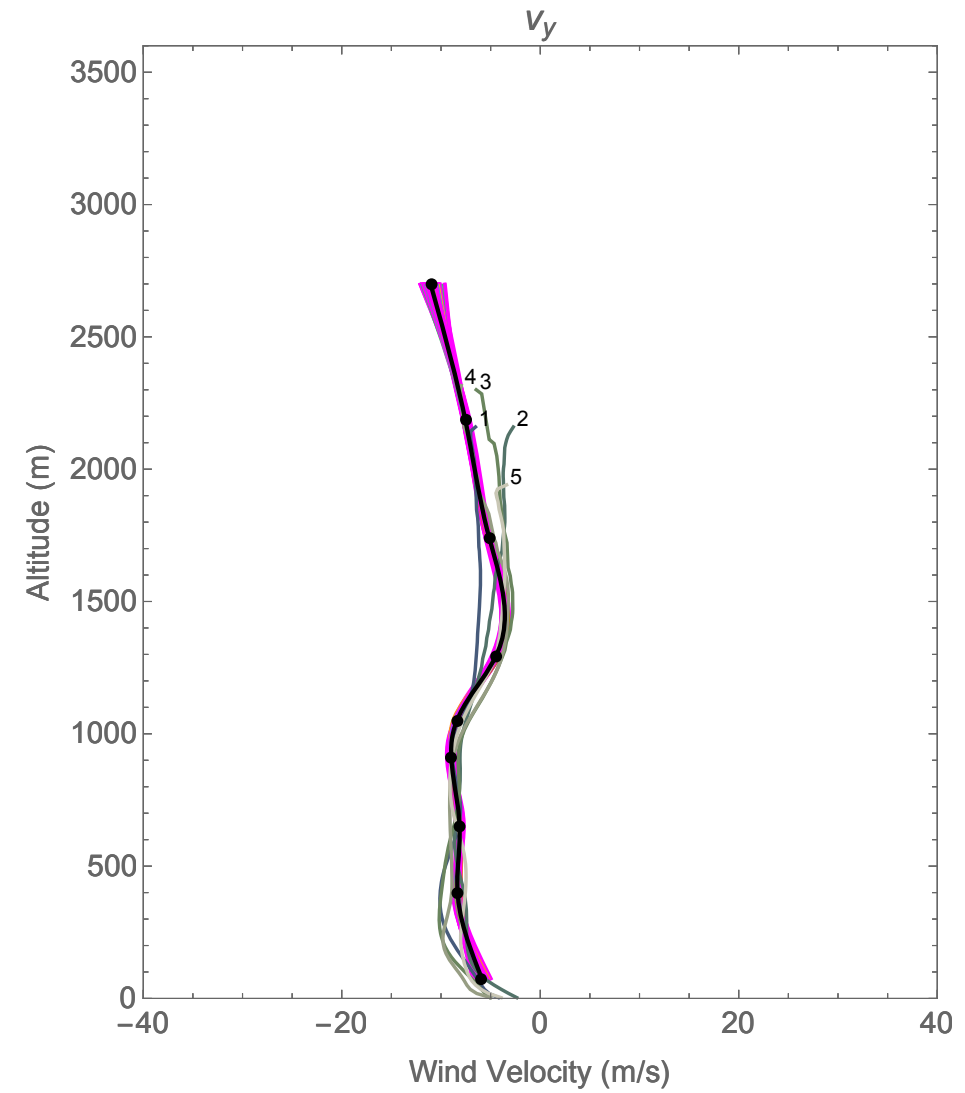
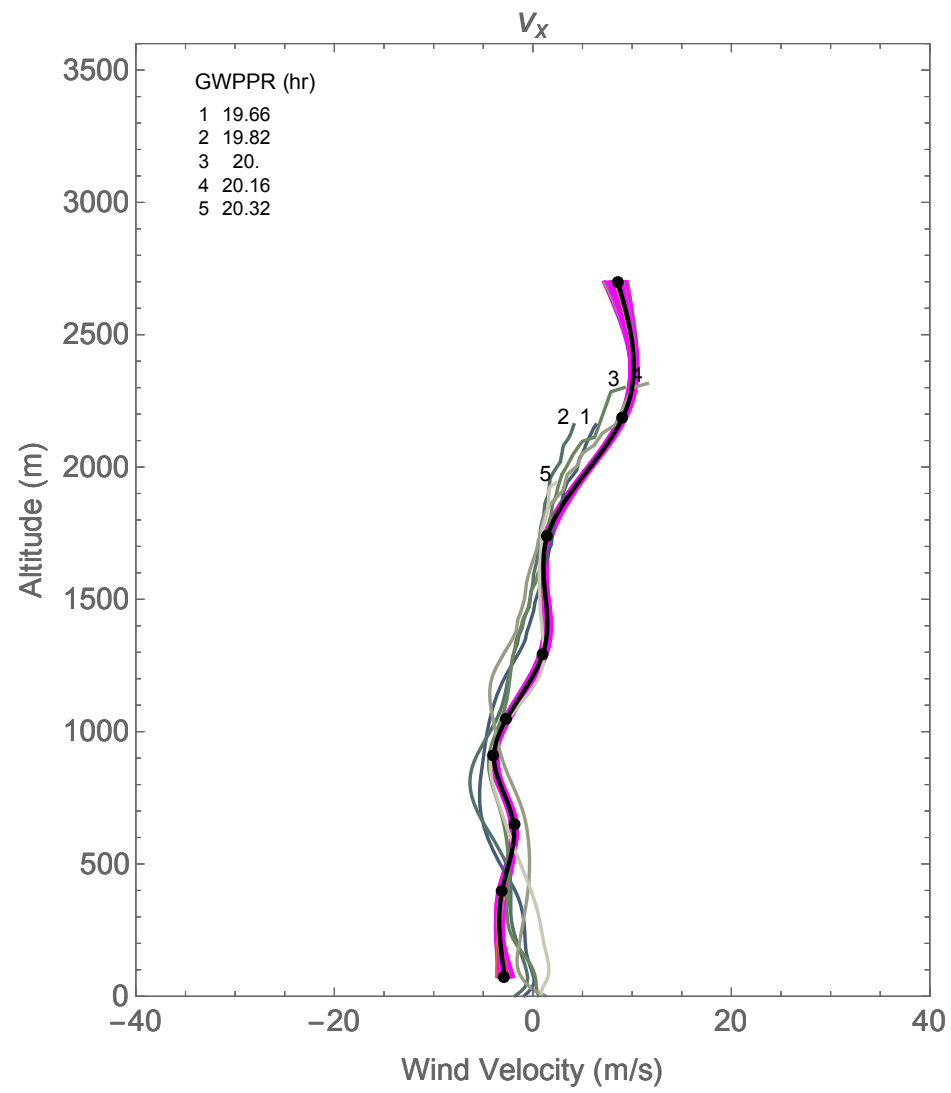
were successfully operating AWiPPR at 3200 m height and 90 m/s speed. Good agreement was achieved between AWiPPR profiles and ground based WiPPR profiles. This fully met our program performance objectives.

Case	Date	Leg	RCV	θ_V^{plane}	ϕ_H^{plane}	Surface	Pattern	z_{avg} (m)	v_{avg} (m/s)	Roll	$\theta_V^{\text{surface}}$	R_{slant}
1	20161014	Leg03	1.5a	29.9	135	water	circles	1546.2	66.6	-26.3	49.8	2396.9
2	20170201	Leg04	1.5a	19.6	135	land	circles	2338.2	70.9	-19.5	34.5	2846.4
3	20170823	Leg06	2	20.	135	land	circles	3055.8	69.8	28.6	17.7	3216.6
4	20170927	Leg02	2	20.	135	land	circles	3148.7	74.7	24.9	15.7	3278.
5	20170927	Leg04	2	20.	135	land	circles	3178.3	89.9	29.3	18.6	3354.9
6	20171025	Leg08	2	20.	135	land	circles	3074.2	67.2	33.2	21.3	3301.6
7	20180205	Leg02	2	10.	135	land	circles	3097.3	86.6	19.5	13.1	3181.
8	20180205	Leg03	2	10.	135	land	circles	3147.4	89.6	29.	22.3	3404.8
9	20180403	Leg02	2	10.	135	land	circles	3223.4	90.3	20.5	14.3	3327.5
10	20180403	Leg06	2	10.	135	land	circles	3226.8	91.3	20.6	14.6	3334.1
11	20180403	Leg12	2	10.	135	land	circles	3244.7	88.8	20.5	14.3	3349.4
12	20180404	Leg02	2	10.	135	land	circles	3233.2	87.8	20.3	13.9	3331.1
13	20180404	Leg06	2	10.	135	land	circles	3126.5	88.1	20.8	14.5	3230.3
14	20180522	Leg04	2	10.	135	land	circles	3206.4	89.6	21.2	15.	3319.6
15	20180522	Leg07	2	10.	135	land	circles	3208.9	91.4	17.6	13.7	3309.7
16	20180522	Leg09	2	10.	135	land	circles	3267.	88.8	20.6	14.4	3373.9

Summary AWiPPR measurements from October 2016 through May 2018.



AWiPPR 2 May 2018 operating at 3200 m and 90 m/s compared to WiPPR measurements.



AWiPPR 4 April 2018 operating at 3200 m and 88 m/s compared to WiPPR measurements.

Reasons for Success

One) We began the project with low-noise, wide dynamic range electronics that were so sensitive that they could measure the variation of sky noise temperature as a function of time of day and radar tilt angle. The atmosphere is colder if you look straight up. Additionally the radar electronics have approximately 80 dB of dynamic range. This allowed us to measure and resolve the large difference in echos between the ground echo and echo from clear air scatter. Over the course of the AWiPPR project, we refined our electronics package through the use of a single side band concept, thereby reducing the noise floor by an additional 3 dB.

Two) We spent the time period 2011-2015 building and refining the WiPPR system. From this we learned in particular that clear air scatter is actually convective turbulence with a point like character that can be tracked as it passes through the radar beam. In the AWiPPR project we built kinematical models of this process. These models eventually enabled us to build a signal processing technique that allowed us to extract slant range and Doppler velocity data from range velocity matrices at 0 dB SNR. We refer to this technique as BayesSummedLogOdds.

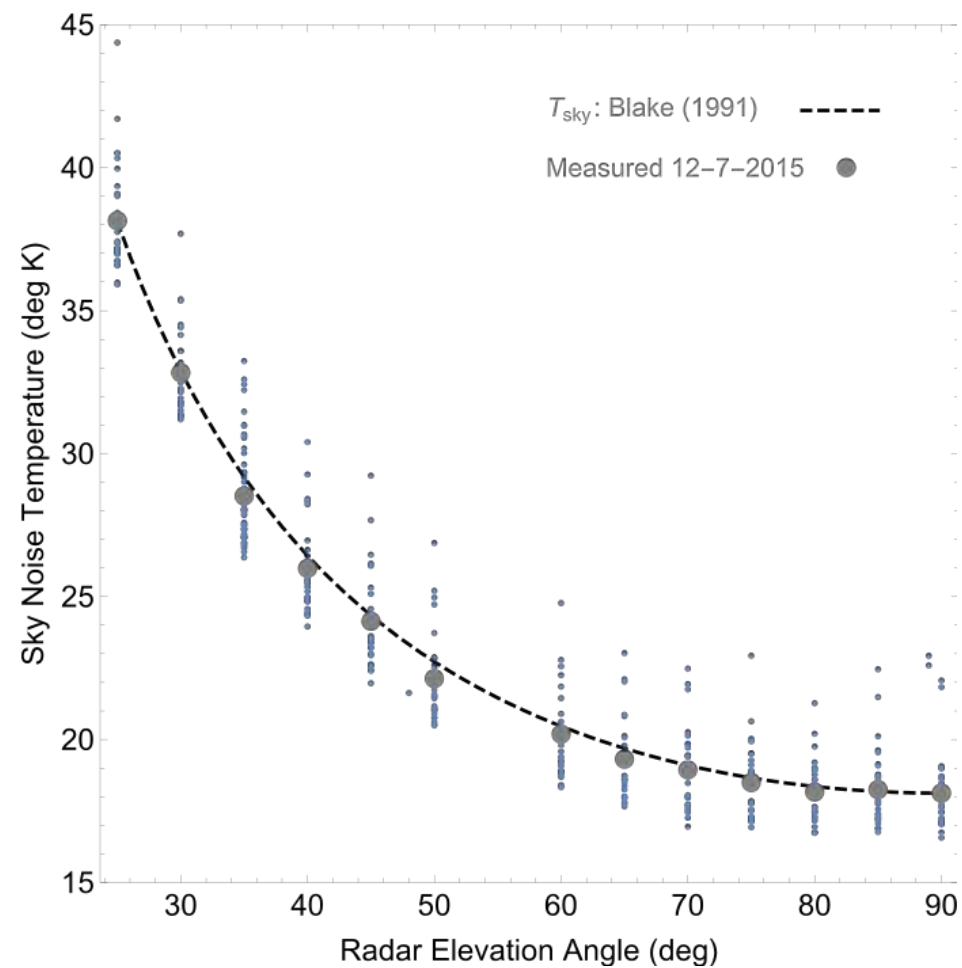
Three) During the WiPPR project we developed an analytic model of the generation, mixing and detection of frequency modulated

signals. For AWiPPR we refined this model and used it to develop a specialized shading scheme for the range Fast Fourier Transforms (FFTs) in the range velocity matrix formation signal process. This shading approach allowed us to detect near ground echos from clear air scatter via suppression of the strong echo from the ground bounce.

Four) We changed our operating tactics. Initially we thought it would be beneficial operate the radar well off vertical in order to reduce ground backscatter. It was actually better to operate closer to vertical and at higher altitudes. This avoided the problem of trying to find clear air echos in the sidelobe structure of the ground bounce echo.

Five) We developed a spline-based approach for estimating wind velocity profiles from slant range-Doppler velocity contacts. We refer to this model as Low Contact Rate Wind Engine (LCRWE). Using LCRWE maximizes the use of sparse data in a physically sensible way that is consistent with Bayesian probability theory. In conjunction with building LCRWE we developed an image based signal process approach that effectively doubled the unambiguous Doppler velocity range of the radar electronics in situations when virga is present. This is very common in southern Mississippi and other locations.

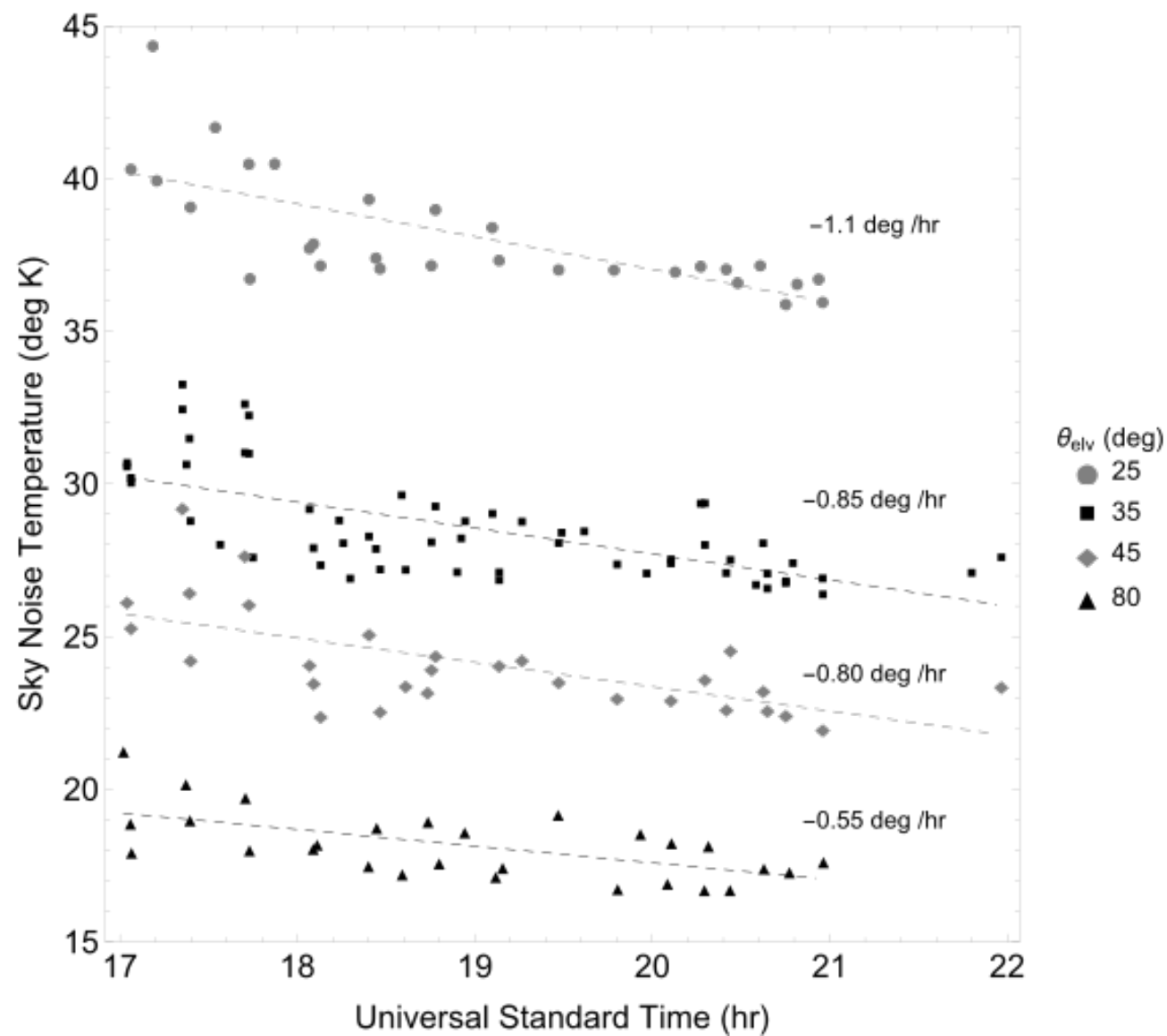
Six) We executed a well thought out test program that supported the above. Additionally we had outstanding engineering support, in particular navigation which is so vital to reconstructing the kinematics and beam pointing directions of a radar mounted on a moving aircraft.



Sky noise observed on 7 December 2015 with the WiPPR system.

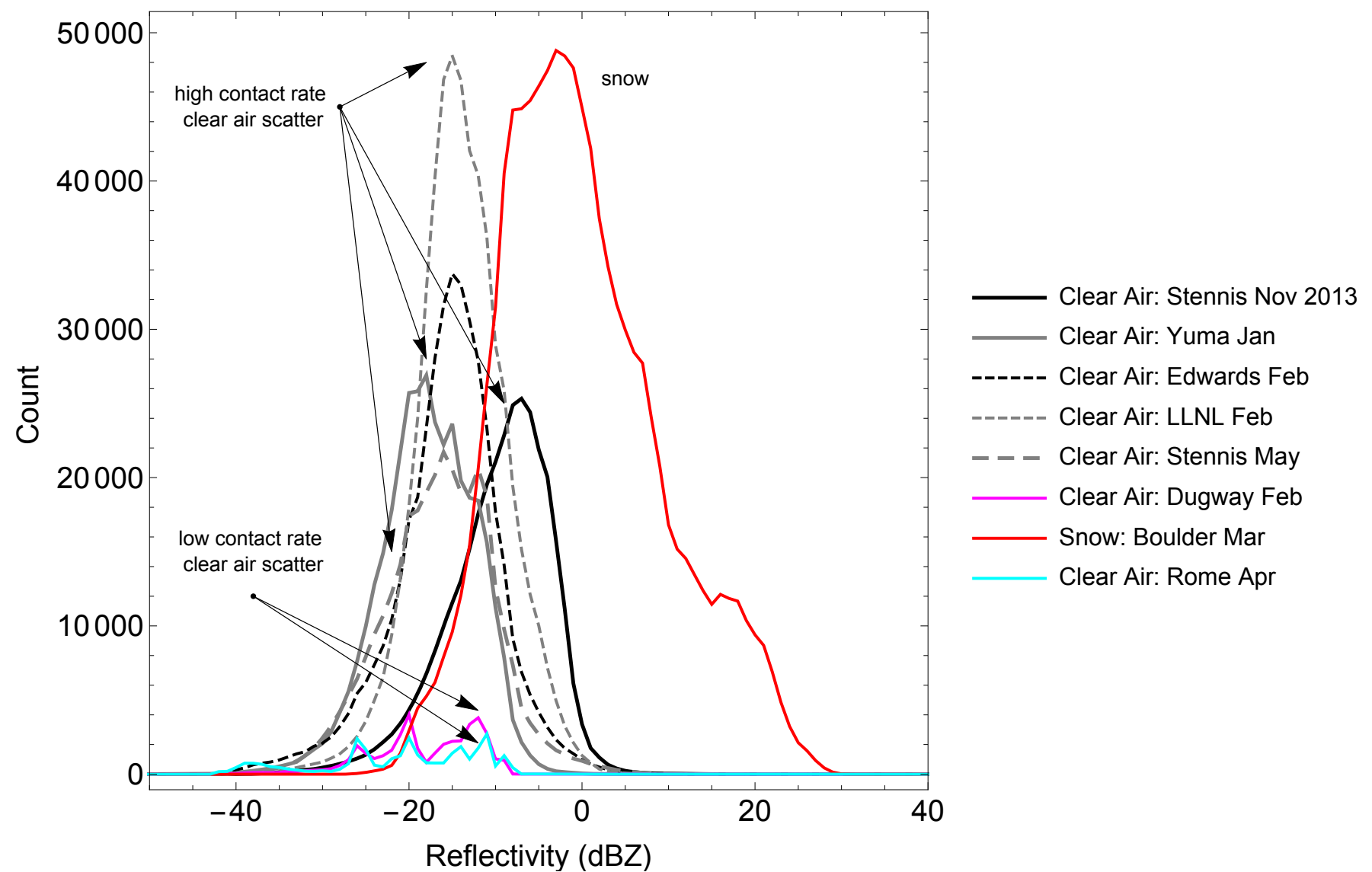
Measured sky noise values made with the WiPPR radar on 7 December 2015 at the Stennis International Airport are shown above. Data were collected from 1658 to 2103 Z. Sky noise is radiation observed by the radar that comes from the troposphere (0-47 km) and the cosmos (beyond 47 km for ordinary radar frequencies). The range of radar elevation angles in the figure is 25-90 degrees with 90 degrees corresponding to the vertical (radar looking straight up). At 33.4 GHz the cosmos contribution to sky noise is 2.5 deg K and is very nearly independent of elevation angle over the range 25-90 deg. Thus sky noise in this case is effectively tropospheric noise. Smaller points in the plot indicate individual radar sky noise measurements. Larger gray points

indicate mean values. Estimations of the sky noise temperature using algorithms from the text *Radar-Range Performance Analysis* (Blake,1991) are shown for reference via the dashed black line. Computations with the Blake algorithms for the sky noise temperature have been made using on scene measurements of atmospheric temperature and pressure. Sky noise temperature is lowest near the vertical because at these angles the radar beam trajectory spends the least amount of time in the denser portions of the atmosphere which occur at lower altitudes. The data in the figure indicate a radar total system noise temperature of 130 deg K at an elevation angle of 90 degrees.



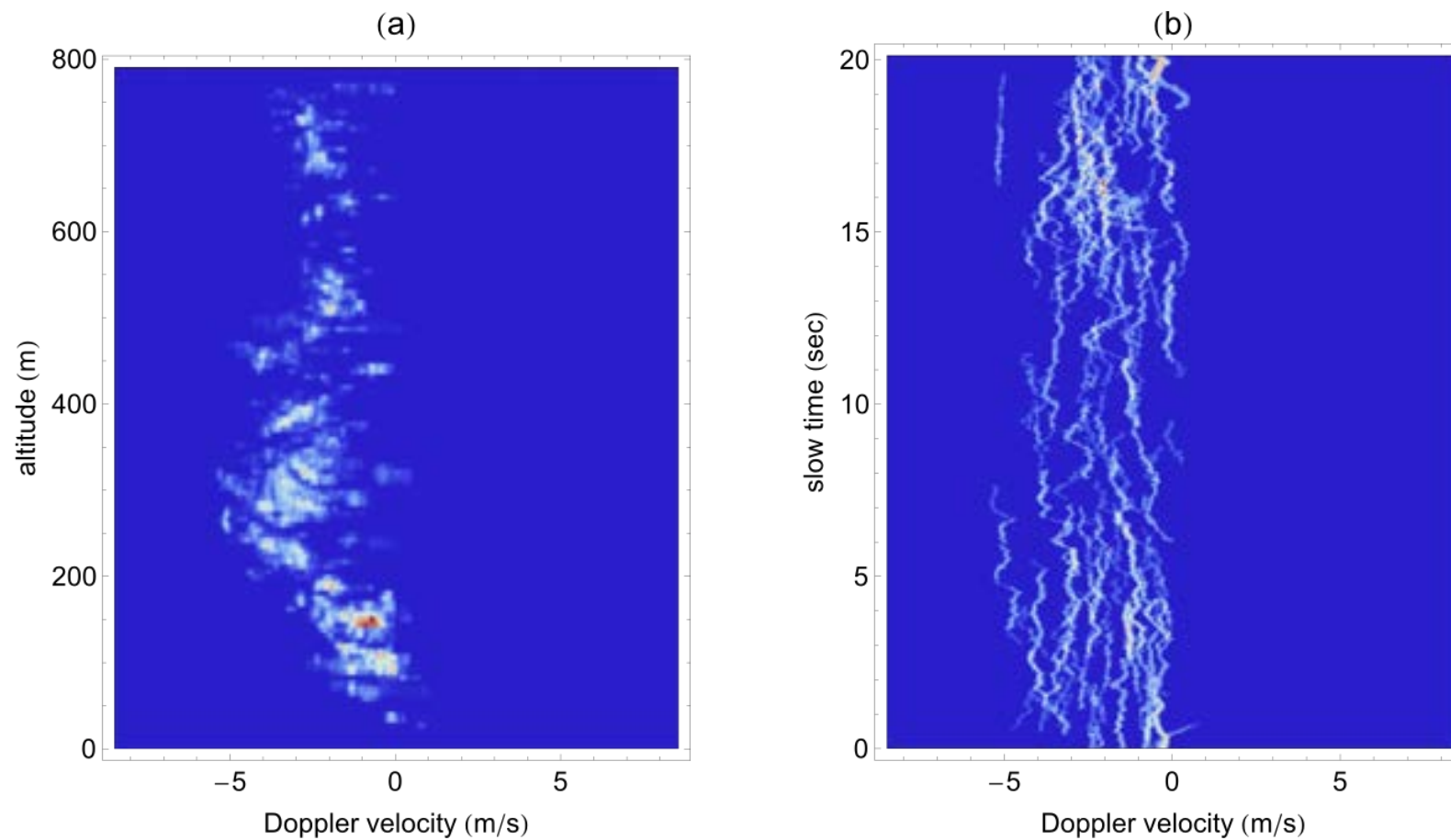
Time variation of sky noise observed on 7 December 2015 with the WiPPR radar.

This figure indicates that the WiPPR radar can track temperature trends in the atmosphere over the course of hours and across multiple tilt angles. Sky noise is also referred to as brightness temperature.



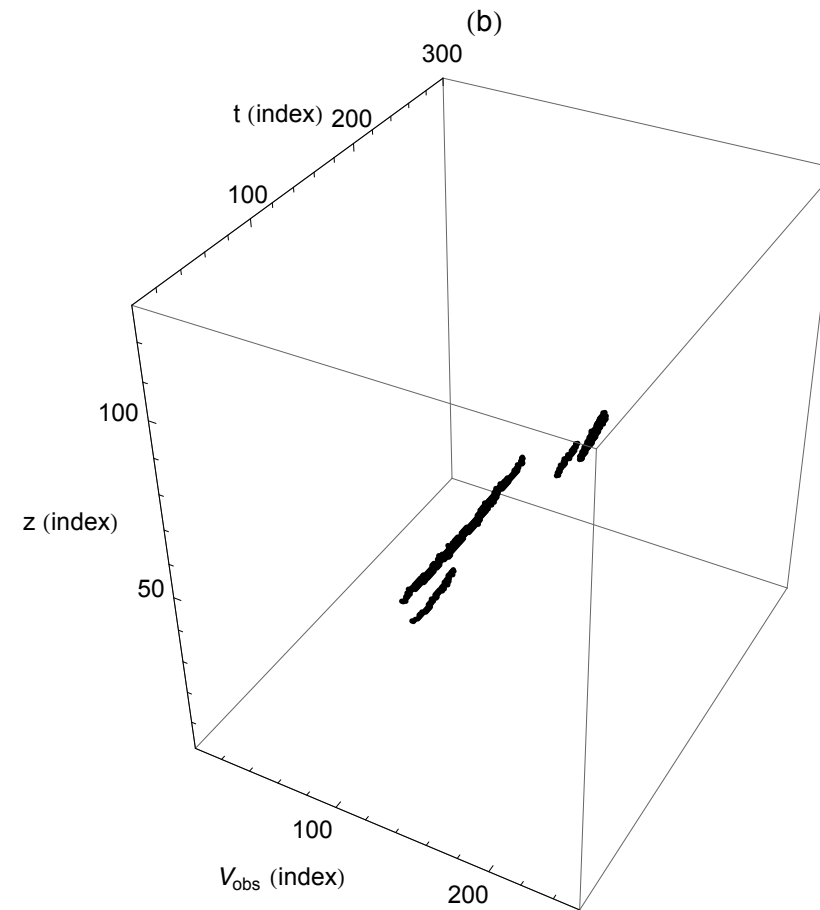
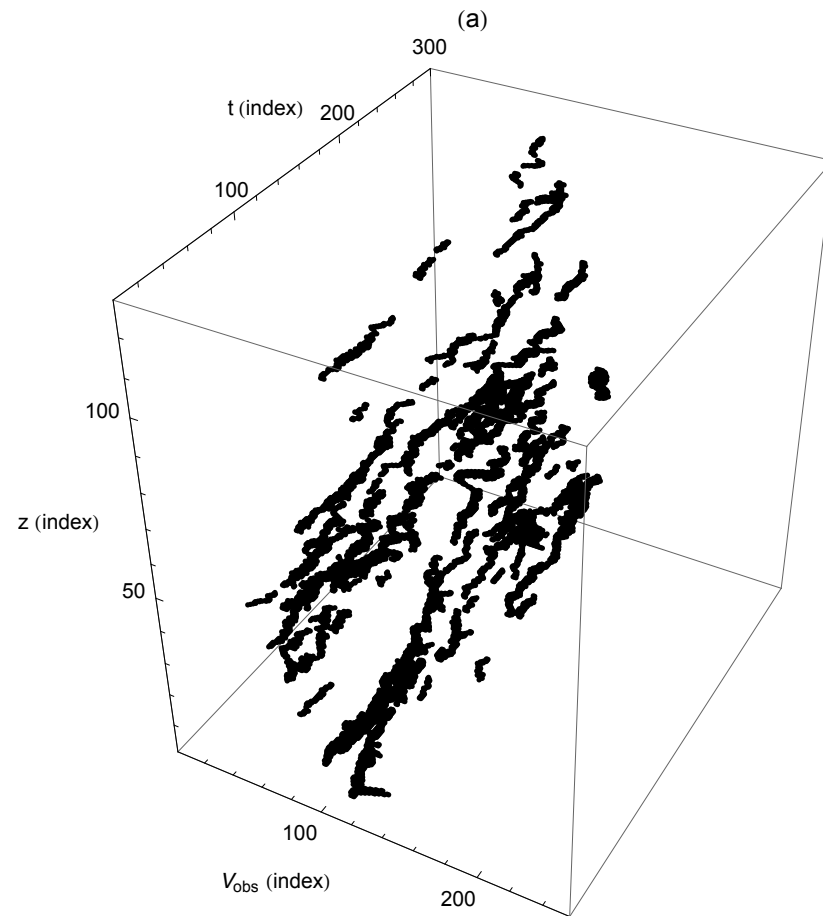
Wide dynamic range of WiPPR radar.

The above figure shows the relationship between the dBZ reflectivity of targets and radar contact count under three conditions: 1) High contact rate clear air scatter (convective turbulence), 2) Low contact rate clear air scatter (most probably mechanically generated turbulence) and 3) snow. The range in dBZ values resolved by the radar is 70 dB indicating the wide dynamic range of the WiPPR radar electronics. This wide dynamic range was a key building-block technology for AWiPPR.



Particle like nature of WiPPR contacts.

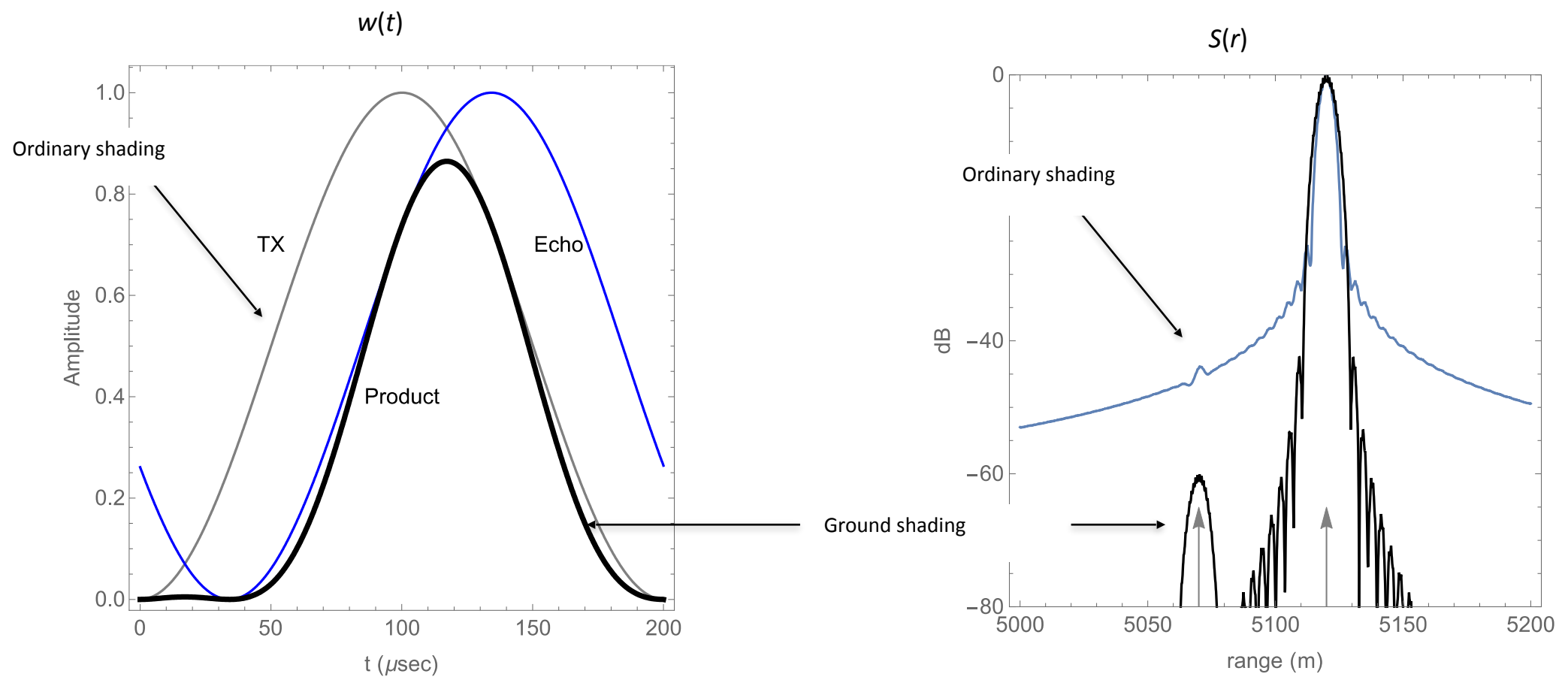
WiPPR measurement of Doppler velocity of the wind using data collected on 27 March 2012 at Yuma AZ under absolutely clear skies. The fundamental quantities that an FMCW radar system measures are the distance, reflectivity and Doppler velocity of objects as they move through the radar beam as a function of time. This produces a 3 dimensional time-range-velocity radar data cube. The time span shown in the figure is 20 sec. If the radar data cube is averaged over time the result is the range velocity matrix (RVM) shown in a). If the data cube is thresholded in SNR and accumulated over altitude the result is the Doppler-time gram shown in b). The tracks moving through image (b) are caused by reflections from turbulence as it moves through the radar beam.



WiPPR data cubes for high and low contact rate clear air scatter from 2012.

A pair of data cubes produced from WiPPR radar data recorded on 27 March 2012 on the Yuma Proving Grounds at a site located about 10 miles south of Quartzsite, AZ. Data cube (a) was produced using data recorded at 12:53 PM local time and data cube (b) was produced using data recorded 6 hours earlier at 6:54 AM. The clear air scatter tracks in both data cubes have been made visible by displaying only those voxels in the data cube with more than 9 dB of signal to noise

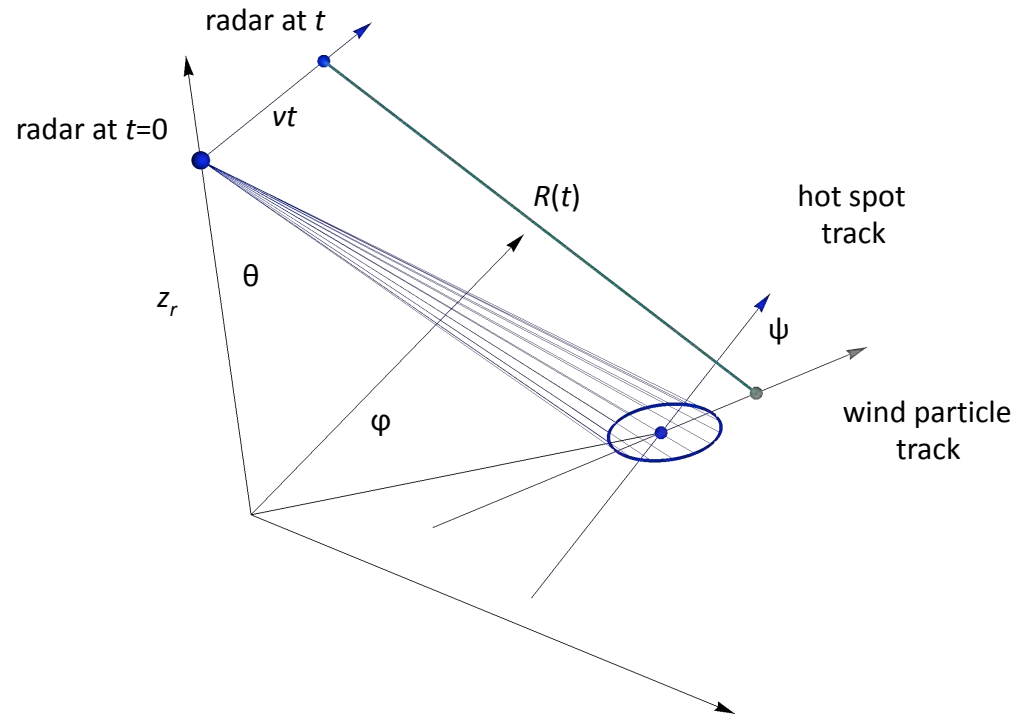
ratio. Morphological processing has also been used to reject any connected features smaller than size 20. The tracks shown in part a and part b result from the radar's ability to track targets in Doppler velocity, time and slant range. In part a, there are 123 tracks that move through the data cube in 20 seconds. In part b, there are 4 tracks that move through the data cube in 20 seconds.



Ground echo suppression for AWiPPR.

Left) Gray curve is Hann shading in the fast-time domain. Blue curve is Hann shading, shifted to the arrival time of the ground echo. Black curve is the product of the gray and blue shading functions. Right) Ordinary Hann shading is compared to the product shading described on the left. The effect is dramatic. The weak echo at about range 5075 meters is made clearly visible. This technique was originally conceived during 2011 in the early stages of our radar program. It was refined for AWiPPR applications.

At time $t=0$ the wind particle passes through the hot spot of the radar beam. $R(t)$ is the instantaneous distance between the radar and the wind particle.



At time $t=0$ the radar and its hotspot are located respectively at $(0,0,z_r)$ and $z_r\{\sin\phi\tan\theta,\cos\phi\tan\theta,0\}$. The radar beam points in the direction $\{\sin\theta\sin\phi,\sin\theta\cos\phi,-\cos\theta\}$.

$$\vec{r}_{radar}(t) = \{0, vt, z_r\}$$

$$\vec{r}_{wind}(t) = \vec{r}_{hot}(0) + ut\{\sin\psi, \cos\psi, 0\}$$

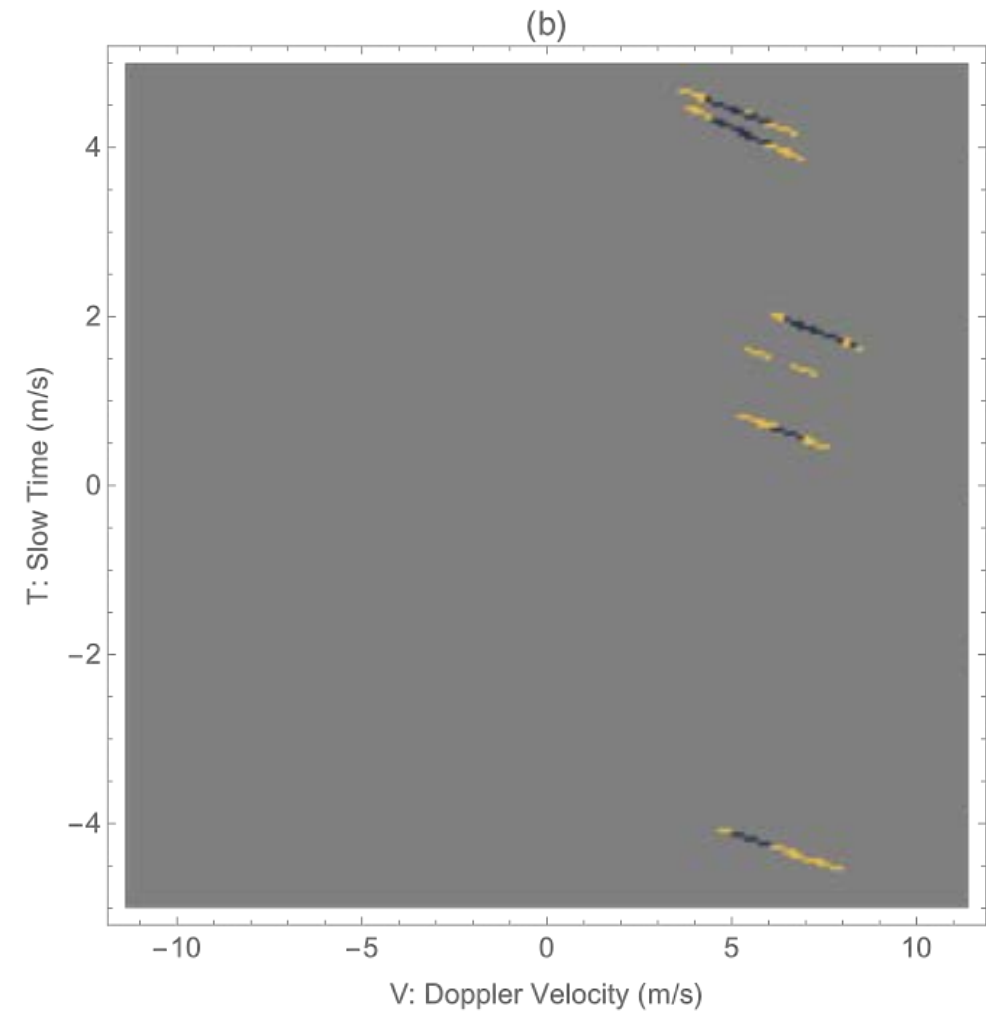
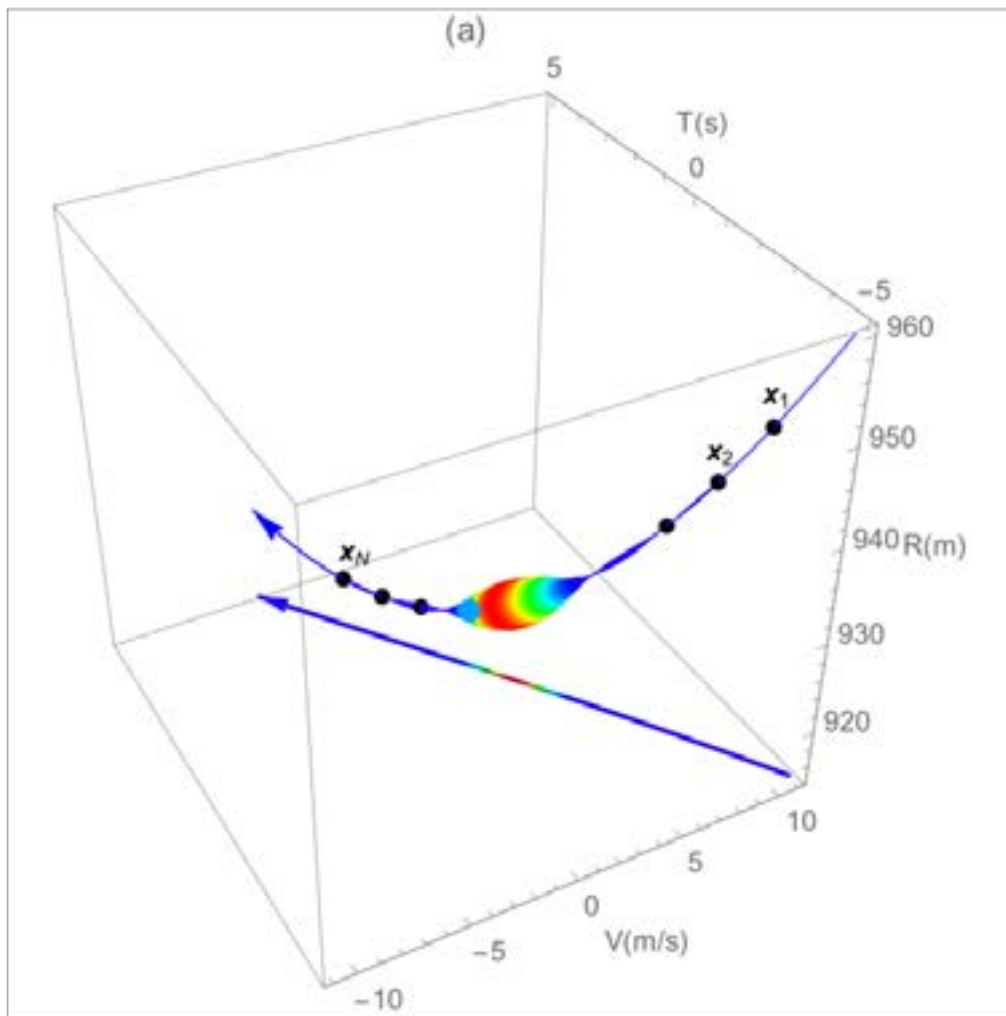
$$R(t) = \left| \vec{r}_{radar}(t) - \vec{r}_{wind}(t) \right|$$

All kinematic quantities of interest can be computed by taking derivatives of $R(t)$. For instance the Doppler velocity of the echo is at time $t=0$

$$V = -\frac{dR(0)}{dt} = -[-v\cos\phi + u\cos(\phi - \psi)]\sin\theta$$

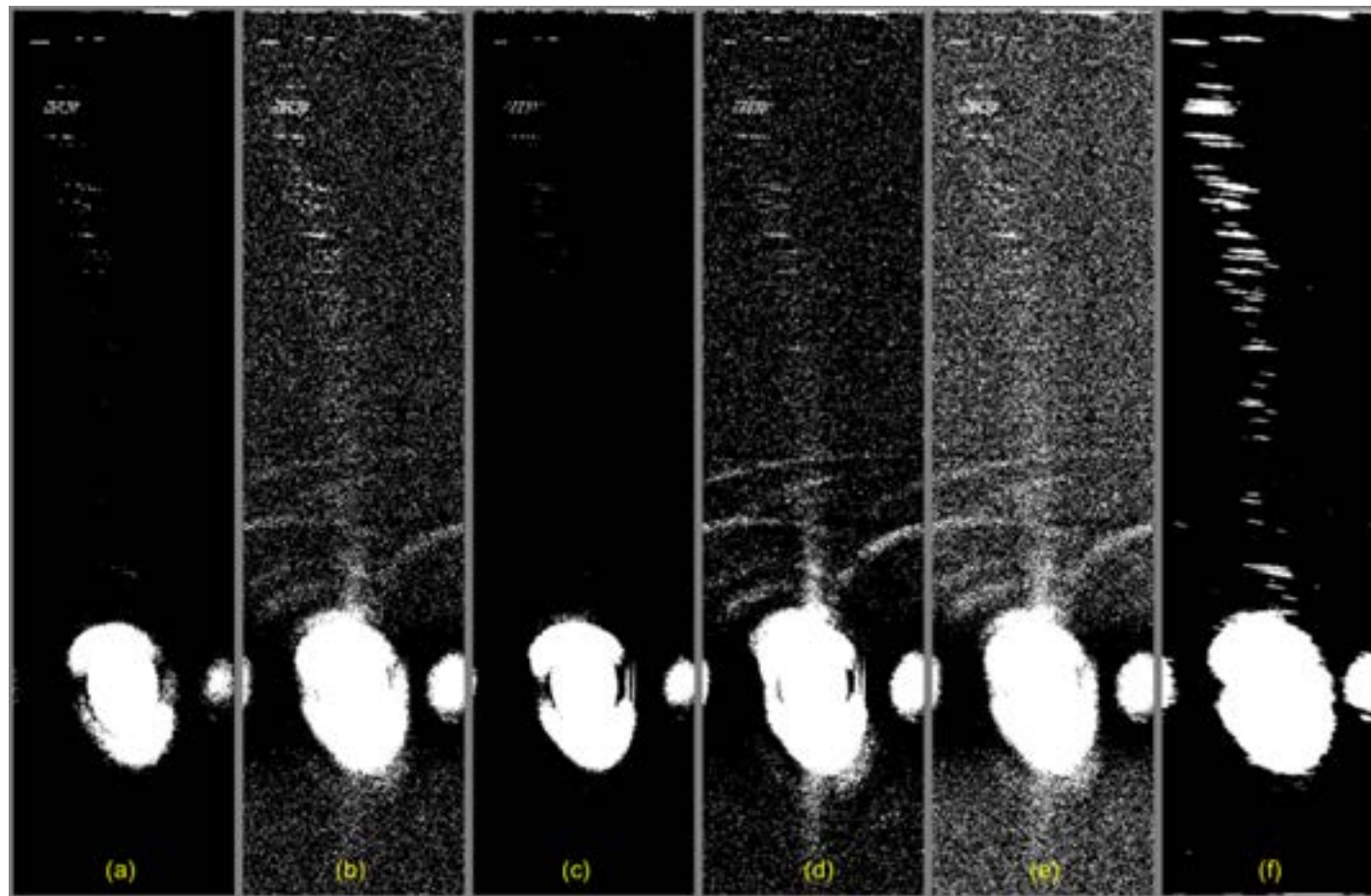
Part 1) AWiPPR 3D particle kinematics.

In the above figure $R(t)$ is the instantaneous distance between the radar and a wind particle that passes through the hot spot of the radar beam at time $t = 0$. Beginning with a knowledge of $R(t)$ we can compute all kinematic quantities of interest including the Doppler velocity $V = -dR/dt$, the Doppler acceleration dV/dT and the related spatial acceleration dV/dR . Each of these three derivatives depend upon the vertical separation z_r , radar speed v , the radar beam azimuthal and vertical directions (ϕ, θ) , the wind speed u and its direction ψ . Collectively these three derivatives define the motion of a radar particle through a Doppler (V), slow time (T) slant range (R) data cube. Any knowledge of $(z_r, v, \theta, \phi, u, \psi)$ constrains particle motion in the VTR data cube presents the possibility for obtaining processing gain against background noise.



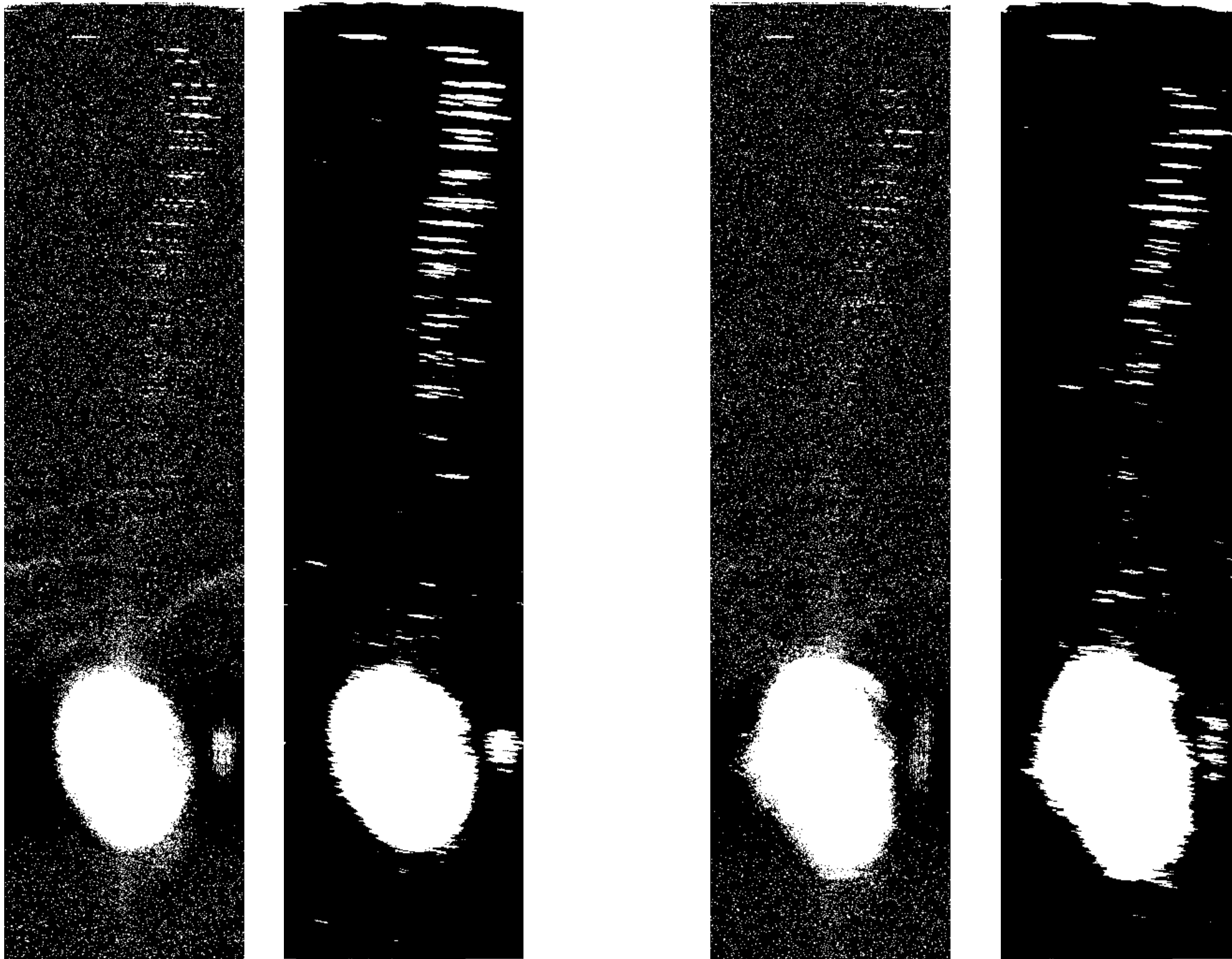
Part 2) AWiPPR 3D particle kinematics.

(a) Particle motion in Doppler (V), slow time (T) and slant range (R) referred to as VTR space. (b) Motion in VT space obtained by marginalization. Both a) and b) incorporate radar beam pattern effects. The key point here is that the Doppler velocity, echo time, slant range and relative echo amplitude of the particle can be predicted and this knowledge can be exploited to produce processing gain.

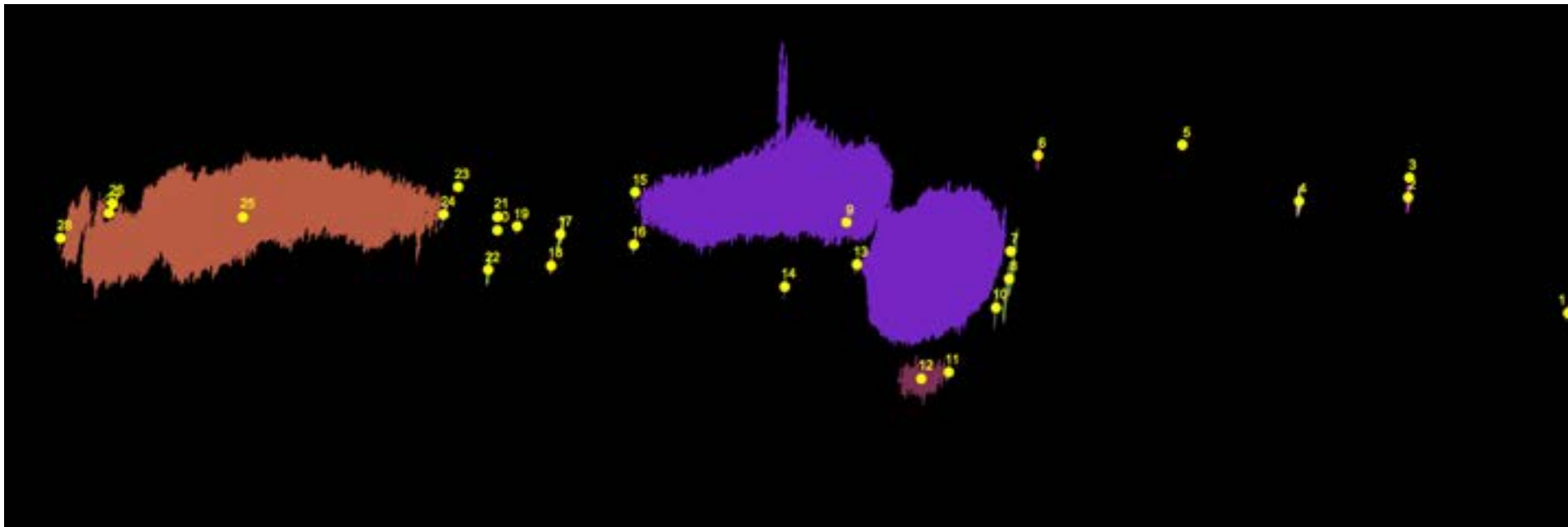
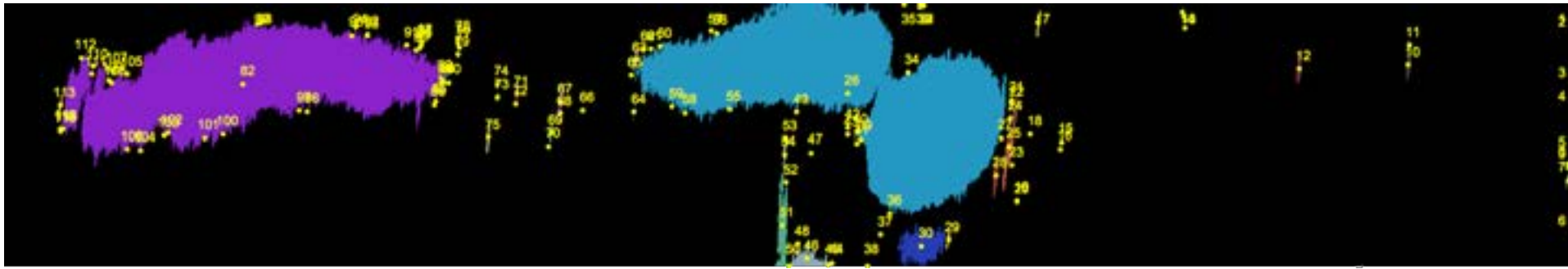


SNR improvements from AWiPPR data cube processing and marginalization.

Various strategies for marginalizing the AWiPPR data cube in order to obtain usable Doppler velocity-slant range information are illustrated in this figure. The radar data cube used here is of size 100 by 1024 by 256. The data is from file 24, leg 03 on 14 October 2016. The radar stack size (number of slow time steps) is 100. The number of slant range cells is 1024 and the number of Doppler velocity cells is 256. Marginalization across the 100 slow time steps produces an image of size 1024 by 256 from which useful information can be extracted. Strategies: (a) Convert the radar data cube to SNR, set a threshold at 15 dB SNR, binarize and sum across slow time. This produces counts. The maximum possible number of counts in case (a) is 100. The upper portion of the Doppler-range profile can be seen in (a) but there are few detections near the ground. (b) Same strategy as (a) but with the SNR threshold reduced to 10 dB. Now we can see a profile but false alarms are serious problem. (c) Partition the radar data cube into 5 blocks each of length 20. Compute averages in for each block, threshold at 5 dB SNR and marginalize across slow time. The maximum possible count in a Doppler-range cell is now 5. This reduces false alarms but there is no capability near the ground. (d) Like (c) but with the SNR threshold reduced to 2 dB. We can see the profile but there are a huge number of false alarms. (e) Adopt a Bayesian approach: Normalize the radar data cube by dividing by the local standard deviation and convert to decibel log odds. Threshold at 5 dB log odds, binarize and marginalize. We can see the profile but there are many false alarms. (f) Bayesian solution based upon the radar cube from (d) and a kinematic particle track prior probability distribution that exploits a priori information about aircraft motion, wind direction and wind speed. The marginalization threshold in the image is 40 dB log odds. The improvement in detection range and low false alarm rate is striking in comparison to parts (a) through (e).

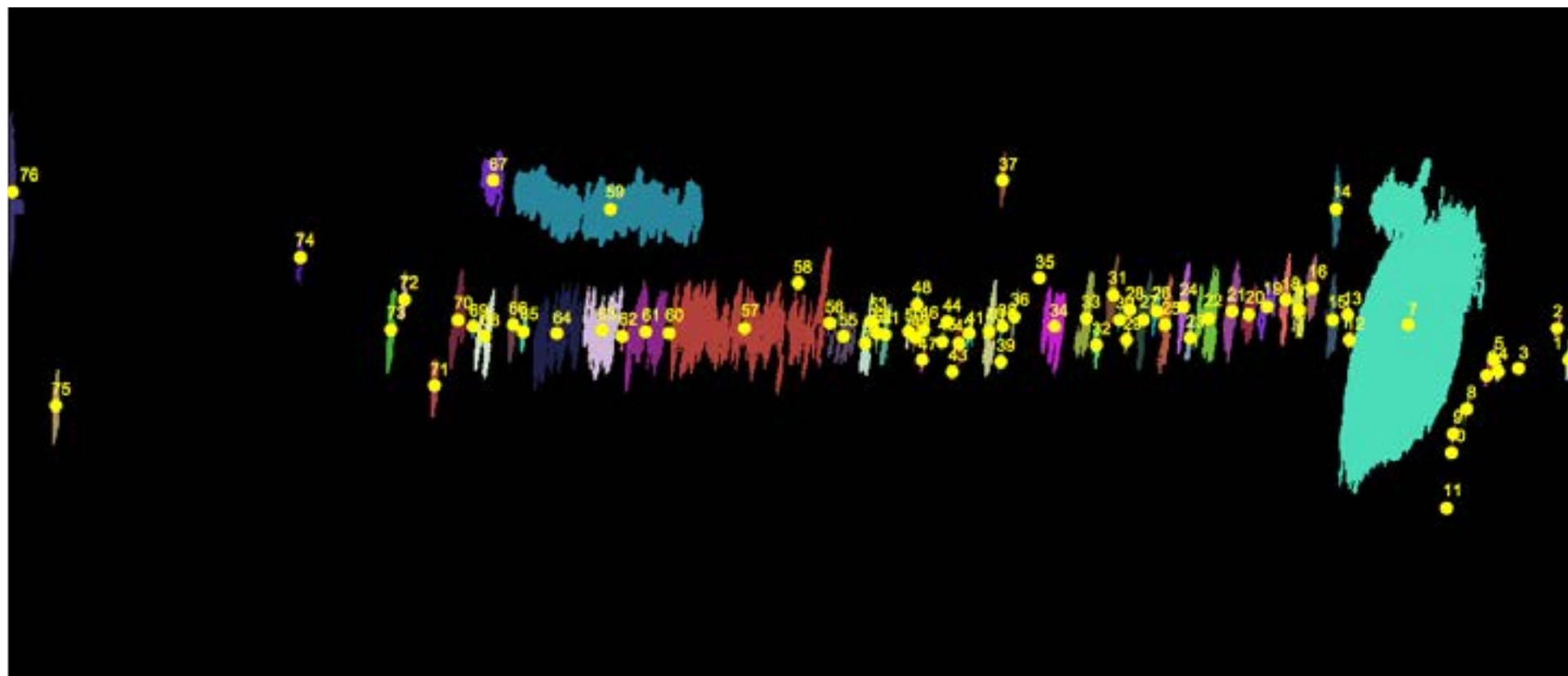
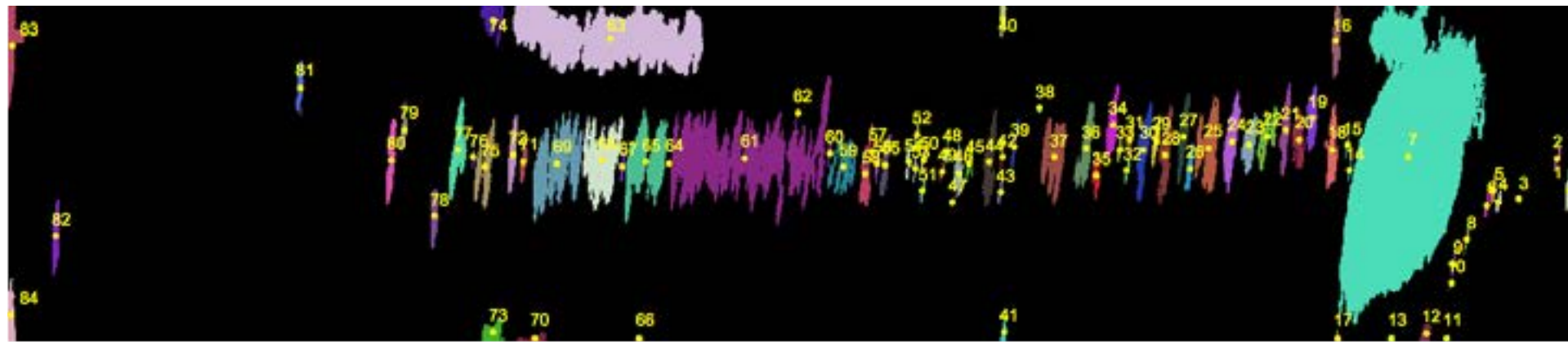


Two examples of the effectiveness of BayesSummedLogOdds processing from October 2016 AWiPPR data.



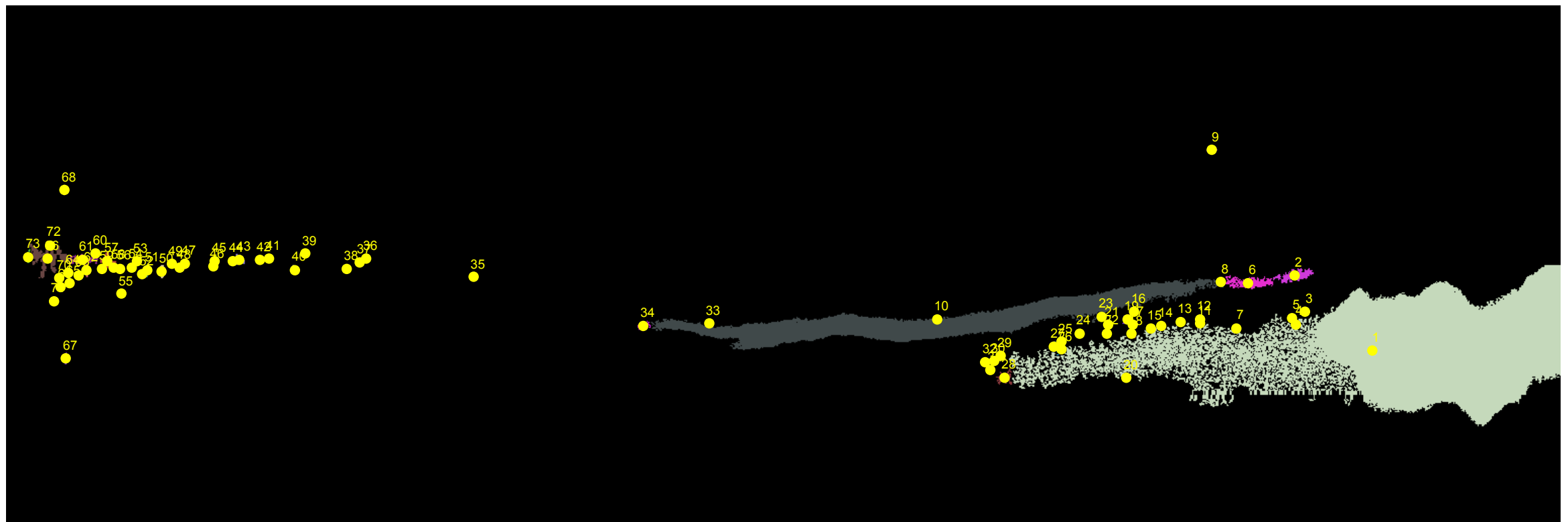
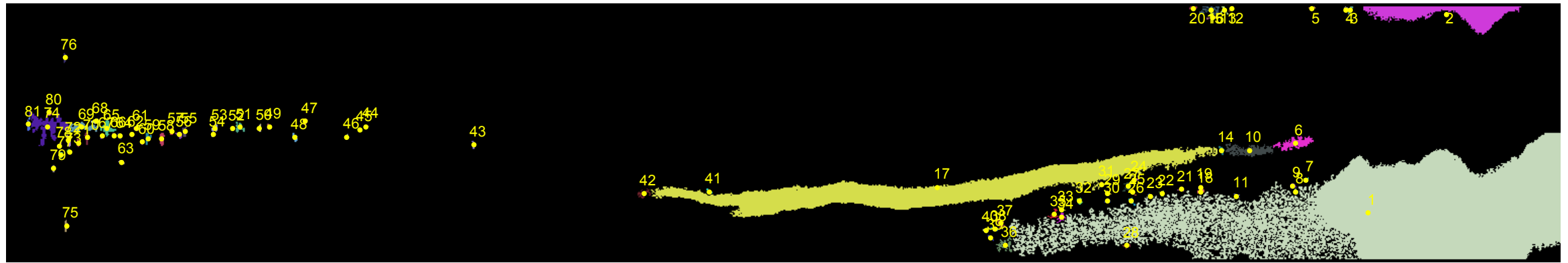
Doppler unwrapping applied to AWiPPR October 2016 data.

The upper image shows the BayesSummedLogOdds image after the application of morphological processing. The lower image shows the results of Doppler unwrapping. The Doppler bandwidth has been doubled. In each image the horizontal axis is slant range and the vertical axis is Doppler velocity. These data were recorded during a time period when the primary contact was falling hydrometers or possibly clouds.



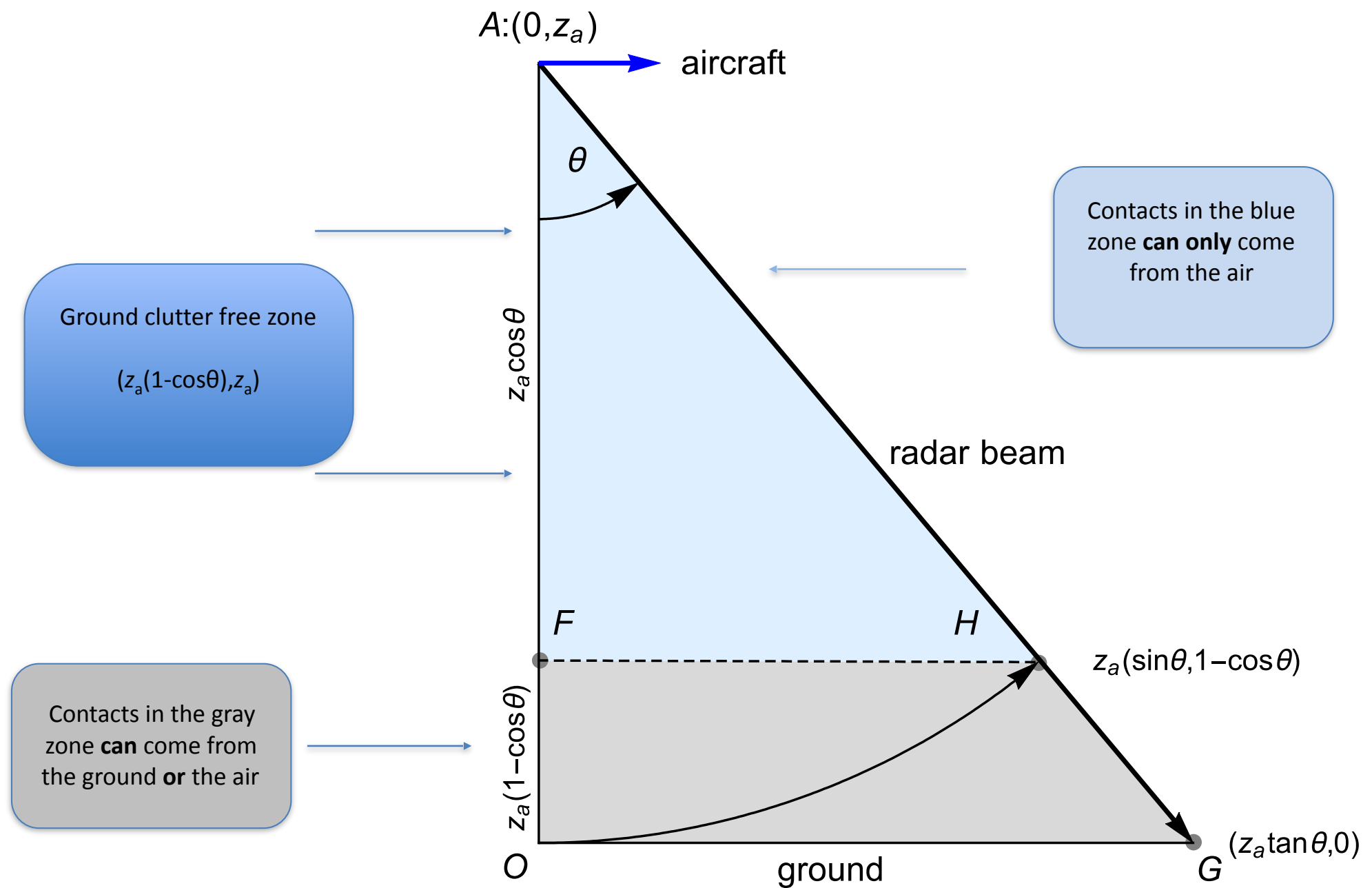
Doppler unwrapping applied to AWiPPR 2018 data.

The upper image shows the BayesSummedLogOdds image after the application of morphological processing. The lower image shows the results of Doppler unwrapping. The Doppler bandwidth has been doubled. In each image the horizontal axis is slant range and the vertical axis is Doppler velocity. The dominant contact in these images is clear air scatter (convective turbulence). There is at least one large and one small virga contact. Morphological feature 7 is the main portion of the ground echo. Feature 37 in the lower image appears to be some type of outlier.



Doppler unwrapping applied to GWiPPR 2017 data.

The upper image shows the BayesSummedLogOdds image after the application of morphological processing. The lower image shows the results of Doppler unwrapping. The Doppler bandwidth has been doubled. In each image the horizontal axis is slant range and the vertical axis is Doppler velocity. The ground is all the way to the left. Altitudes increase from left to right. The images are a rich mix of clear air contacts and contacts from hydrometers. The algorithm does a beautiful job of resolving the high altitude hydrometer feature (number 1 in the lower image) and correctly representing its Doppler velocity.



Ground clutter outlier filtering.

Contacts in the altitude range $(0, z_a(1 - \cos(\theta)))$ where z_a is the altitude of the aircraft can come from the ground or the air. By operating at near vertical angles the altitude interval corresponding to the gray colored region can be minimized in extent.

Representing the Wind with Splines

- At the onset of the AWiPPR program we knew that we needed a technique that would correctly estimate a wind velocity profile beneath an aircraft from what we thought might be a minimal number of Doppler velocity contacts produced by the radar. The tool that we chose for doing this was the natural cubic spline.
- The Doppler velocities measured by the radar during the AWiPPR maneuver and the spline ordinates for the wind vector velocity profile beneath the aircraft are related by a linear relationship referred to as the forward equation:

$$\mathbf{V}_{obs} = \mathbf{A} \cdot \mathbf{f}$$
- The least squares solution to this equation can be easily found provided that the matrix $\mathbf{A}^T \mathbf{A}$ is not ill conditioned.
- In the illustration shown to the right there are 15 measured Doppler values and a spline with 4 pivot points.
- The altitude of the first spline pivots must be the altitude of the lowest Doppler contact. The altitude of the last spline pivots must be the altitude of the highest Doppler contact.
- The altitudes of the remaining spline pivots are found by requiring equal amounts of Doppler data in the resulting altitude bands. They can also be user selected.
- The matrix \mathbf{A} is a complicated function of contact altitudes, beam pointing directions and spline constraints.
- The size of the matrix \mathbf{A} in the example is 15 by 4x3=12.

$$\vec{V}_{obs} = \mathbf{A} \vec{f}$$

$$\begin{pmatrix} V_1 \\ V_2 \\ V_3 \\ V_4 \\ V_5 \\ V_6 \\ V_7 \\ V_8 \\ V_9 \\ V_{10} \\ V_{11} \\ V_{12} \\ V_{13} \\ V_{14} \\ V_{15} \end{pmatrix} = \begin{pmatrix} a_{1,1} & a_{1,2} & a_{1,3} & a_{1,4} & a_{1,5} & a_{1,6} & a_{1,7} & a_{1,8} & a_{1,9} & a_{1,10} & a_{1,11} & a_{1,12} \\ a_{2,1} & a_{2,2} & a_{2,3} & a_{2,4} & a_{2,5} & a_{2,6} & a_{2,7} & a_{2,8} & a_{2,9} & a_{2,10} & a_{2,11} & a_{2,12} \\ a_{3,1} & a_{3,2} & a_{3,3} & a_{3,4} & a_{3,5} & a_{3,6} & a_{3,7} & a_{3,8} & a_{3,9} & a_{3,10} & a_{3,11} & a_{3,12} \\ a_{4,1} & a_{4,2} & a_{4,3} & a_{4,4} & a_{4,5} & a_{4,6} & a_{4,7} & a_{4,8} & a_{4,9} & a_{4,10} & a_{4,11} & a_{4,12} \\ a_{5,1} & a_{5,2} & a_{5,3} & a_{5,4} & a_{5,5} & a_{5,6} & a_{5,7} & a_{5,8} & a_{5,9} & a_{5,10} & a_{5,11} & a_{5,12} \\ a_{6,1} & a_{6,2} & a_{6,3} & a_{6,4} & a_{6,5} & a_{6,6} & a_{6,7} & a_{6,8} & a_{6,9} & a_{6,10} & a_{6,11} & a_{6,12} \\ a_{7,1} & a_{7,2} & a_{7,3} & a_{7,4} & a_{7,5} & a_{7,6} & a_{7,7} & a_{7,8} & a_{7,9} & a_{7,10} & a_{7,11} & a_{7,12} \\ a_{8,1} & a_{8,2} & a_{8,3} & a_{8,4} & a_{8,5} & a_{8,6} & a_{8,7} & a_{8,8} & a_{8,9} & a_{8,10} & a_{8,11} & a_{8,12} \\ a_{9,1} & a_{9,2} & a_{9,3} & a_{9,4} & a_{9,5} & a_{9,6} & a_{9,7} & a_{9,8} & a_{9,9} & a_{9,10} & a_{9,11} & a_{9,12} \\ a_{10,1} & a_{10,2} & a_{10,3} & a_{10,4} & a_{10,5} & a_{10,6} & a_{10,7} & a_{10,8} & a_{10,9} & a_{10,10} & a_{10,11} & a_{10,12} \\ a_{11,1} & a_{11,2} & a_{11,3} & a_{11,4} & a_{11,5} & a_{11,6} & a_{11,7} & a_{11,8} & a_{11,9} & a_{11,10} & a_{11,11} & a_{11,12} \\ a_{12,1} & a_{12,2} & a_{12,3} & a_{12,4} & a_{12,5} & a_{12,6} & a_{12,7} & a_{12,8} & a_{12,9} & a_{12,10} & a_{12,11} & a_{12,12} \\ a_{13,1} & a_{13,2} & a_{13,3} & a_{13,4} & a_{13,5} & a_{13,6} & a_{13,7} & a_{13,8} & a_{13,9} & a_{13,10} & a_{13,11} & a_{13,12} \\ a_{14,1} & a_{14,2} & a_{14,3} & a_{14,4} & a_{14,5} & a_{14,6} & a_{14,7} & a_{14,8} & a_{14,9} & a_{14,10} & a_{14,11} & a_{14,12} \\ a_{15,1} & a_{15,2} & a_{15,3} & a_{15,4} & a_{15,5} & a_{15,6} & a_{15,7} & a_{15,8} & a_{15,9} & a_{15,10} & a_{15,11} & a_{15,12} \end{pmatrix} \begin{pmatrix} f_{x,1} \\ f_{x,2} \\ f_{x,3} \\ f_{x,4} \\ f_{y,1} \\ f_{y,2} \\ f_{y,3} \\ f_{y,4} \\ f_{z,1} \\ f_{z,2} \\ f_{z,3} \\ f_{z,4} \end{pmatrix}$$

$$\vec{f}_{LS} = (\mathbf{A}^T \mathbf{A})^{-1} \mathbf{A}^T \vec{V}_{obs} \longleftarrow \text{Least squares estimate of spline pivot points}$$

In the above example there are 15 observed Doppler velocities at 15 corresponding altitudes. Not indicated are the associated radar beam pointing directions. The user has chosen to use 4 pivot points. The unknowns are the spline ordinates. The v_x portion of the wind profile passes through the spline pivots $((z_1, f_{x,1}), (z_2, f_{x,2}), (z_3, f_{x,3}), (z_4, f_{x,4}))$. The v_y portion of the wind profile passes through the spline pivots $((z_1, f_{y,1}), (z_2, f_{y,2}), (z_3, f_{y,3}), (z_4, f_{y,4}))$ and similarly for the v_z portion of the wind profile.

z_{AGL} (m)	beam	$V_{Doppler}$ (m/s)	cosX	cosY	cosZ
175.12	8	-2.44349	0.214577	0.326467	-0.92053
175.373	18	1.86202	0.232198	0.258317	-0.93774
175.86	25	0.600157	-0.170544	-0.307252	-0.936222
175.979	5	3.66389	0.0971597	-0.414543	-0.904828
176.441	27	0.435761	0.0141133	0.336454	-0.941594
.....
2298.05	61	0.936709	-0.279598	-0.180056	-0.943083
2298.95	51	-7.23027	0.291569	-0.224389	-0.929858
2299.71	57	1.88126	-0.335102	0.0662381	-0.93985
2299.79	20	-5.19696	0.0135771	-0.37448	-0.927136
2299.99	47	-6.93572	0.229338	-0.295167	-0.927513

Small portion of an AWiPPR Doppler contact catalog.

The AWiPPR data catalog is very similar in concept to a data catalog from astrophysics but simpler. All information required for wind velocity estimation is in this table. The first column is the echo height above ground level. The second column is a pointer to a BayesSummedLogOdds range velocity matrix. The third column is the Doppler velocity of the clear air scatter contact. Columns 4-6 are the beam pointing direction of the radar beam on which the Doppler contact occurred. Data in the catalog are sorted by altitude. If the user chose to use a spline with 7 pivot points then the abscissa's of the first and last spline pivot s would be $z_1 = 175.12$ and $z_7 = 2299.99$. Spline abscissas z_2 to z_6

would normally be found by requiring equal amounts of Doppler data in the 6 altitude intervals (z_1, z_2) , (z_2, z_3) to (z_6, z_7) . This normally produces a tighter spacing of pivots near the ground than at higher altitudes.

If we form the matrix \mathbf{B} whose rows are the negatives of the directions cosines in columns 4-6 and form the vector \mathbf{V}_{obs} of all of the observed Doppler data in column 3 of the contact table then

$$\mathbf{v}_{avg} = (\mathbf{B}^T \mathbf{B})^{-1} \cdot \mathbf{B}^T \cdot \mathbf{V}_{obs}$$

is an estimate of the average wind velocity over the min-max altitude range in the data catalog.

A Primer on Cubic Splines

The construction of a cubic spline representation for a function $f(z)$ that represents one of the vector components of the wind field begins with representing the second derivative of the function $f(z)$ as a piecewise continuous linear function. This is equivalent to saying that the second derivative representation has a polygonal shape. The approach that we take here is adapted from (von der Linden, 2014). With reference to the accompanying figure suppose that we are given the functional values (z_j, f_j) and additionally the second derivative values m_j . The points (z_j, f_j) will be called control points (or pivot points) and N is the number of control points. The z_j and f_j are respectively referred to as abscissas and ordinates. The spacings between the abscissa points are $h_{j+1} = z_{j+1} - z_j$. They need not be equal.

If $S''(z)$ denotes the second derivative representation of $f(z)$ then integrating $S''(z)$ twice with respect to z yields a cubic representation function in z named $S(z)$ which is known as a

cubic spline. The important property of a cubic spline is that its global curvature over the interval (z_1, z_N) is smaller than the curvature of any other twice continuously differentiable function that passes through the control points (z_j, f_j) provided that we require $S(z)$ to satisfy the boundary conditions $S''(z_1) = S''(z_N) = 0$. We could also achieve minimization in global curvature by assigning the first derivatives of $S(z)$ particular values at the endpoints of the interval (z_1, z_N) . Specifically we could require that $S'(z_1) = f'_1$ and $S'(z_N) = f'_N$.

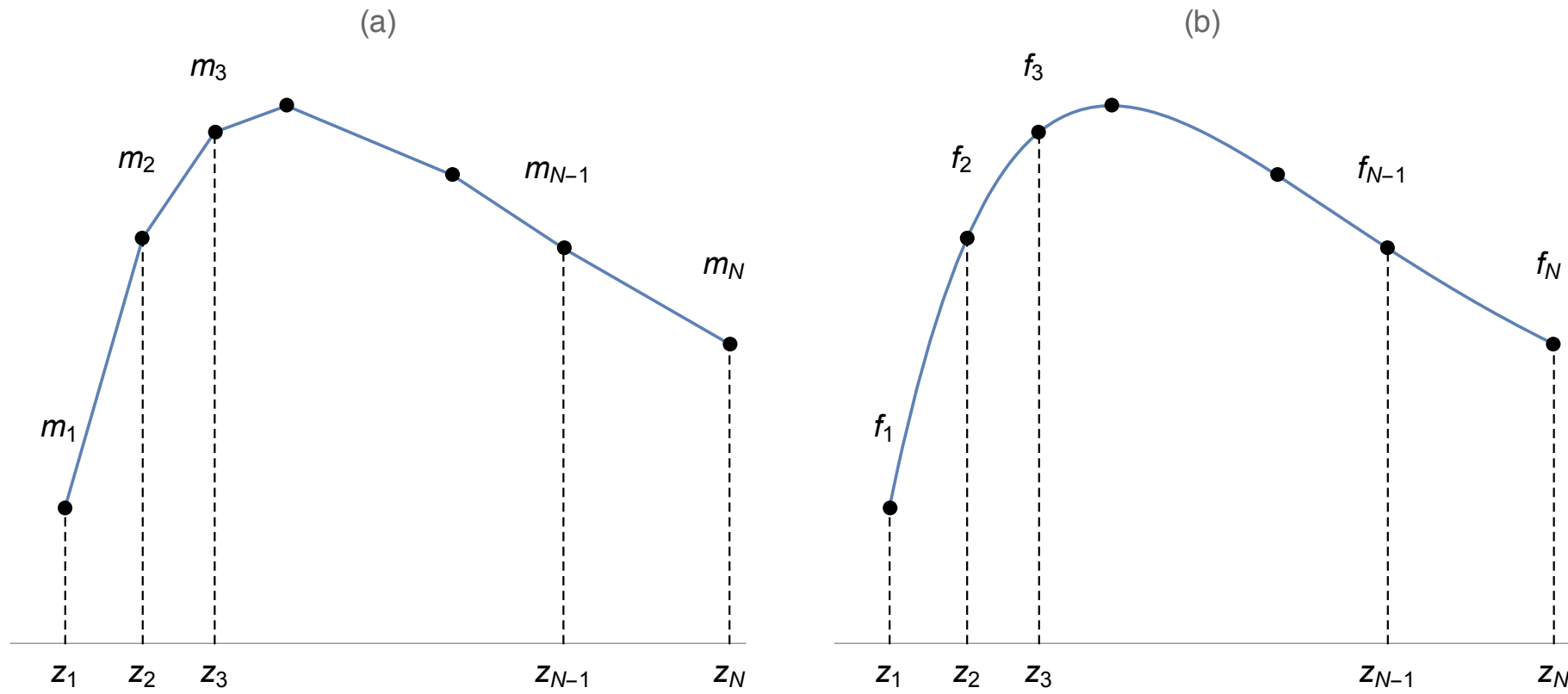
The requirement that $S''(z_1) = S''(z_N) = 0$ produces what is known as a natural cubic spline. This is the case that we will focus on. For a natural cubic spline we have at once that $m_1 = 0$ and $m_N = 0$. The second derivative of $S(z)$ on the interval can be written as the linear function

$$S''(z) = m_j + \frac{m_{j+1} - m_j}{h_{j+1}}(z - z_j) = \frac{z_{j+1} - z}{h_{j+1}}m_j + \frac{z - z_j}{h_{j+1}}m_{j+1}$$

If we integrate $S''(z)$ twice then we have

$$S(z) = \frac{(z_{j+1} - z)^3}{6h_{j+1}}m_j + \frac{(z - z_j)^3}{6h_{j+1}}m_{j+1} + P_j(z - z_j) + Q_j$$

Since $S(z)$ must pass through the control points (z_j, f_j) and (z_{j+1}, f_{j+1}) we immediately have the following relations:



a) The second derivative of the smooth function $S(z)$ is linear within intervals and continuous across intervals. b) Integrating twice yield the function $S(z)$ characterized by the control point abscissa-ordinate pairs (z_j, f_j) .

$$f_j = \frac{1}{6}h_{j+1}^2 m_j + Q_j$$

$$Q_j = f_j - \frac{1}{6}h_{j+1}^2 m_j$$

$$f_{j+1} = \frac{1}{6}h_{j+1}^2 m_{j+1} + P_j h_{j+1} + Q_j$$

$$P_j = \frac{1}{h_{j+1}}(f_{j+1} - f_j) - \frac{1}{6}h_{j+1}(m_{j+1} - m_j)$$

The result is two equations in two unknowns. They can be solved to yield

We can now write $S_j(z)$ in terms of the second derivatives m_j and the control point ordinates f_j . The result is

$$S_j(z) = S_j^{(1)} + S_j^{(2)} + S_j^{(3)}$$

$$S_j^{(1)}(z) = \frac{m_{j+1}h_{j+1}^2}{6} \left[\left(\frac{z - z_j}{h_{j+1}} \right)^3 - \left(\frac{z - z_j}{h_{j+1}} \right) \right]$$

$$S_j^{(2)}(z) = \frac{m_j h_{j+1}^2}{6} \left[\left(\frac{z_{j+1} - z}{h_{j+1}} \right)^3 + \left(\frac{z - z_j}{h_{j+1}} \right) - 1 \right]$$

$$S_j^{(3)}(z) = f_{j+1} \left(\frac{z - z_j}{h_{j+1}} \right) + f_j \left(\frac{z_{j+1} - z}{h_{j+1}} \right)$$

At this point in our derivation the spline pivot abscissas z_j and their spacings h_j are assumed to be known. The values of the pivot point ordinates f_j and their second derivatives m_j remain to be related to one another.

Continuity of the first derivatives of $S_j(z)$ at the control points (z_j, f_j) for $j = 2, 3, \dots, N - 1$ supplies $N - 2$ equations. The additional requirement that second derivative of $S(z)$ is zero at the endpoints (z_1, z_N) supplies two more. This last pair of requirements ensures that we produce a natural cubic spline. At

this point we have the following information about the cubic spline:

$$m_1 = 0$$

$$\frac{h_j}{6} m_{j-1} + \frac{h_j + h_{j+1}}{3} m_j + \frac{h_{j+1}}{6} m_{j+1} = \frac{f_{j+1} - f_j}{h_{j+1}} - \frac{f_j - f_{j-1}}{h_j}$$

$$m_N = 0$$

where the center equation holds for $j = 2, 3, \dots, N - 1$.

At this point it is convenient switch to matrix notation and define $\mathbf{m} = (m_1, m_2, \dots, m_N)^T$ and $\mathbf{f} = (f_1, f_2, \dots, f_N)^T$. The foregoing system of equations can now be written in the matrix form

$$\mathbf{Mm} = \mathbf{Ff}$$

The matrix \mathbf{M} is non-singular. So our system of equations has solution

$$\mathbf{m} = \mathbf{M}^{-1} \mathbf{Ff}$$

which relates the values of the second derivatives in the spline to the values of of the spline at the control point ordinates.

At this point it is convenient to make use of a radar Doppler contact data catalog that is very similar in concept to a data

catalog from astrophysics but simpler. All information required for wind velocity estimation is in this table. The first column is the echo height above ground level denoted by ξ_i for $i = 1, 2, \dots, N_d$ where N_d is the number of data points. The second column is a pointer to a range velocity matrix. The third column is the Doppler velocity of the clear air scatter contact denoted by V_i . Columns 4-6 are the beam pointing direction of the radar beam on which the Doppler contact occurred. These last items are denoted by $\boldsymbol{\eta}_i = (\cos X_i, \cos Y_i, \cos Z_i)$. Data in the catalog are sorted by altitude.

The values of the first and last abscissas of the control points must be $z_1 = \xi_1$ and $z_N = \xi_{N_d}$. The remaining spline abscissas are normally found by requiring equal amounts of Doppler data in the altitude intervals (z_1, z_2) to (z_{N-1}, z_N) . This normally produces a tighter spacing of control points near the ground than at higher altitudes. At a minimum, each of the abscissa intervals (z_j, z_{j+1}) must be populated by at least one of the data abscissa values ξ_j . This prevents singular matrices in the linear algebra that follows.

If the observed data abscissa ξ_i lies in the spline abscissa interval (z_j, z_{j+1}) and if the spline $f(z)$ represents a good fit to the observed Doppler data then it should be approximately true that

$$V_i = S_j^{(1)}(\xi_i) + S_j^{(2)}(\xi_i) + S_j^{(3)}(\xi_i)$$

But since it is the case that $\mathbf{m} = \mathbf{M}^{-1}\mathbf{F}\mathbf{f}$, the measured Doppler value V_i can be written in the form

$$V_i = b_{i1}f_1 + b_{i2}f_2 + \dots + b_{iN}f_N$$

where the coefficients b_{ij} depend on on the data altitudes ξ_i , the control point abscissas z_j and the beam pointing directions $\boldsymbol{\eta}_i = (\cos X_i, \cos Y_i, \cos Z_i)$. This leads at one to the vector equation

$$\mathbf{V}_{obs} = \mathbf{B}\mathbf{f}$$

where \mathbf{V}_{obs} is the vector of observed Doppler velocities and \mathbf{B} is a matrix whose rows are $(b_{i1}, b_{i2}, \dots, b_{iN})$. The foregoing equation is the forward relationship between the observed Doppler data and the control point ordinates of the natural cubic spline. If the square matrix $\mathbf{B}^T\mathbf{B}$ is not ill-conditioned then the least squares solution to the set of over-determined equations is given by

$$\mathbf{f}_{LS} = (\mathbf{B}^T\mathbf{B})^{-1}\mathbf{B}^T\mathbf{V}_{obs}$$

We now turn our attention to obtaining a joint spline representation for the vector wind profile $(v_x(z), v_y(z), v_z(z))$. The relationship between an observed Doppler velocity V_i at altitude ξ_i , the corresponding wind velocity $\mathbf{v}(\xi_i) = (v_x(\xi_i), v_y(\xi_i), v_z(\xi_i))$ and the beam pointing direction $\boldsymbol{\eta}_i$ at that altitude is

$$V_i = -\boldsymbol{\eta}_i \cdot \mathbf{v}(\xi_i)$$

$$\mathbf{F}_{N \times N} = \begin{bmatrix} 0 & 0 & 0 & 0 & \dots & \dots & 0 \\ \frac{1}{h_2} & -\frac{h_2+h_3}{h_2 h_3} & \frac{1}{h_3} & 0 & 0 & & \\ 0 & \frac{1}{h_3} & -\frac{h_3+h_4}{h_3 h_4} & \frac{1}{h_4} & 0 & \dots & 0 \\ \dots & \dots & \dots & \dots & \dots & \dots & \dots \\ 0 & \dots & \dots & 0 & \frac{1}{h_{N-1}} & -\frac{h_{N-1}+h_N}{h_{N-1} h_N} & \frac{1}{h_N} \\ 0 & 0 & 0 & 0 & \dots & 0 & 0 \end{bmatrix}$$

$$\mathbf{M}_{N \times N} = \frac{1}{6} \begin{bmatrix} 2h_2 & 0 & 0 & 0 & \dots & \dots & 0 \\ h_2 & 2(h_2+h_3) & h_3 & 0 & 0 & & \\ & h_3 & 2(h_3+h_4) & h_4 & 0 & \dots & 0 \\ \dots & \dots & \dots & \dots & \dots & \dots & \dots \\ 0 & \dots & \dots & 0 & h_{N-1} & 2(h_{N-1}+h_N) & h_N \\ 0 & 0 & 0 & 0 & \dots & 0 & 2h_N \end{bmatrix}$$

Forms for the matrices \mathbf{F} and \mathbf{M} for the scalar spline problem. For the vector spline problem these matrices generalize to $3N \times 3N$ matrices with a repeated and right-shifted banded form.

The three scalar components of the wind velocity ($v_x(z)$, $v_y(z)$, $v_z(z)$) can be represented by splines with control points $(z_j, f_j^{(x)})$, $(z_j, f_j^{(y)})$ and $(z_j, f_j^{(z)})$ where $j = 1, 2, \dots, N$.

In light of the information matrix \mathbf{B} defined in the previous section we can write

$$V_i = -\eta_i^{(x)} T_i^{(x)} - \eta_i^{(y)} T_i^{(y)} - \eta_i^{(z)} T_i^{(z)}$$

where

$$T_i^{(x)} = b_{i1} f_1^{(x)} + b_{i2} f_2^{(x)} + \dots + b_{iN} f_N^{(x)}$$

$$T_i^{(y)} = b_{i1} f_1^{(y)} + b_{i2} f_2^{(y)} + \dots + b_{iN} f_N^{(y)}$$

$$T_i^{(z)} = b_{i1} f_1^{(z)} + b_{i2} f_2^{(z)} + \dots + b_{iN} f_N^{(z)}$$

This can be written in the compact matrix form

$$\mathbf{V}_{obs} = \mathbf{A}\mathbf{f}$$

where \mathbf{A} is a $N_d \times 3N$ matrix and where \mathbf{f} is now defined to be the $3N \times 1$ vector of spline ordinates

$$\mathbf{f} = (f_1^{(x)}, f_2^{(x)}, \dots, f_N^{(x)}, f_1^{(y)}, f_2^{(y)}, \dots, f_N^{(y)}, f_1^{(z)}, f_2^{(z)}, \dots, f_N^{(z)})^T$$

The least squares solution for \mathbf{f} is

$$\mathbf{f}_{LS} = (\mathbf{A}^T \mathbf{A})^{-1} \mathbf{A}^T \mathbf{V}_{obs}$$

The likelihood of the spline ordinates $L(\mathbf{V}_{obs} | \mathbf{f})$ can be written in the form (apart from a factor of $(2\pi)^{-N_d/2}$)

$$\sigma_V^{-N_d} \exp\left[-\frac{RSS}{2\sigma_V^2}\right] \exp\left[-\frac{(\mathbf{f} - \mathbf{f}_{LS})^T \mathbf{A}^T \mathbf{A} (\mathbf{f} - \mathbf{f}_{LS})}{2\sigma_V^2}\right]$$

where σ_V is the error we make in measuring Doppler velocity and

$$RSS = (\mathbf{V}_{obs} - \mathbf{A}\mathbf{f}_{LS})^T (\mathbf{V}_{obs} - \mathbf{A}\mathbf{f}_{LS})$$

is the residual sum of squares. The matrix

$$\mathbf{F}_{Fisher} = \sigma_V^{-2} \mathbf{A}^T \mathbf{A}$$

is the Fisher information (or precision) matrix of the measurement. Large Doppler measurement errors make for low precision. The inverse of the Fisher information matrix is the covariance matrix

$$\mathbf{\Sigma} = \sigma_V^2 (\mathbf{A}^T \mathbf{A})^{-1}$$

The covariance matrix represents the error with which we estimate the wind velocity. The square roots of the three diagonal elements of the covariance matrix are the standard deviations associated with the least squares estimate of the spline ordinates.

In most circumstances we do not know the Doppler measurement error σ_V . An estimate of its value is

$$\sigma_V^2 = \frac{1}{D - 3N} RSS$$

In the above equation we divide by $D - 3N$ because $3N$ parameters have been estimated from the data.

Reference: *Bayesian Probability Theory* by Wolfgang von der Linden, Volker Dose and Udo von Toussaint, Cambridge University Press 2014.

Checks on the Wind Inversion Process

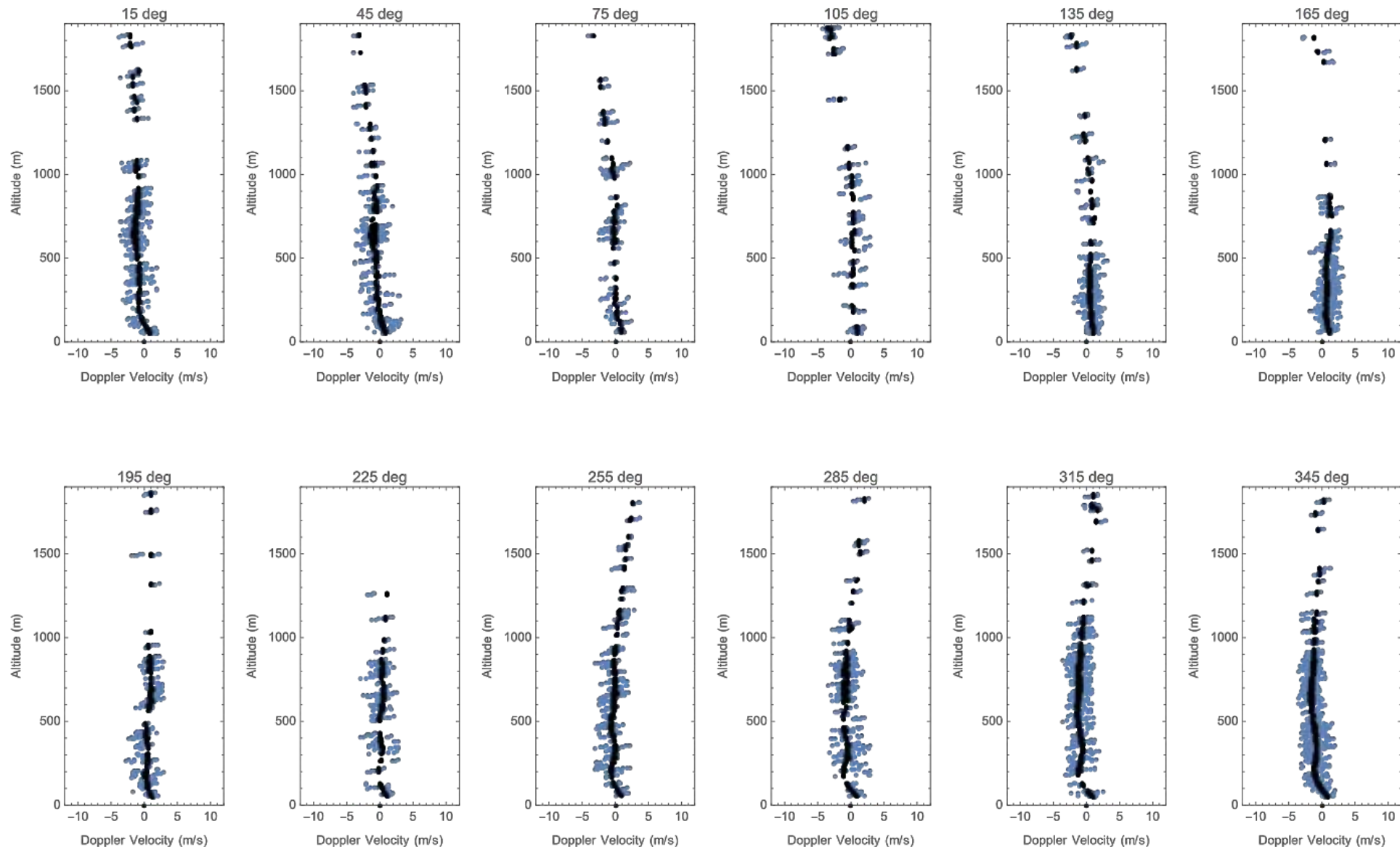
We consider three checks on the wind inversion process in this section. Examples of comparisons of LCRWE estimates to measurements from a trusted system have already been presented.

First) The inversion process estimates the wind velocity profile $(v_x(z), v_y(z), v_z(z))$ from the observed Doppler data. Given a wind velocity estimate, we can predict the Doppler beam velocities. Predicted and measured Doppler velocities should agree. Suppose V is a Doppler velocity at some altitude z in the contact catalog and that $(\cos X, \cos Y, \cos Z)$ is the corresponding beam pointing direction from the catalog. Then if $(v_{spl,x}, v_{spl,y}, v_{spl,z})$ is the corresponding spline estimate of wind velocity at altitude z it must be the case that

$$V \approx - (\cos X, \cos Y, \cos Z) \cdot (v_{spl,x}, v_{spl,y}, v_{spl,z})$$

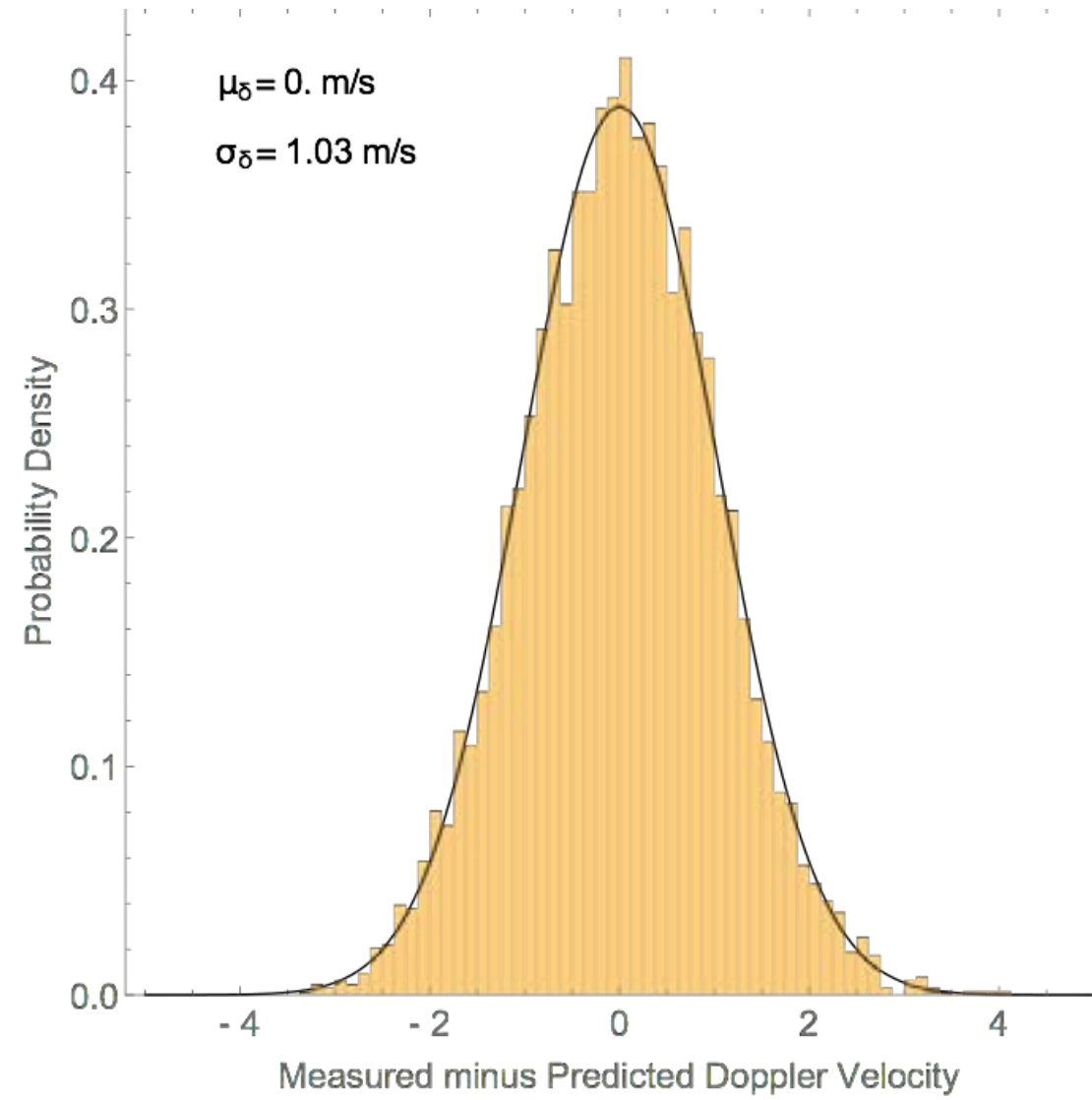
Two) The inversion process assumes that the Doppler velocity data is measured subject to Gaussian errors. This implies that the residuals should follow a normal distribution. If there are no systematic effects in the inversion, then the distribution of residuals should have zero mean.

Three) The mean wind speed estimated by the procedure should be in general agreement with the method of intervals (simple least squares estimates over altitude intervals).



Check 1) Comparison of measured an predicted Doppler data from an AWiPPR measurement.

Measured data (blue) dots is presented in 12 azimuthal directions each 30 deg apart. Black dots are the projection of the wind profile onto the radar beams. This is done on a point by point basis for each contact in the data catalog.



Check 2) Distribution of residual errors closely fits a Gaussian probability density function with zero mean.

The method of intervals provides a sanity check on the inversion process in situations where there is a great deal of Doppler data.

The solid points in the plot to the right are the spline pivot points. The smooth lines are the splines themselves. The wind profile is represented by a spline with seven pivot points.

The horizontal lines are the error bounds of the spline pivots.

In situations where there is an abundance of AWiPPR Doppler velocity data, wind velocity can be estimated by a simple technique. We refer to this approach as the method of intervals and its results are indicated by the open squares.

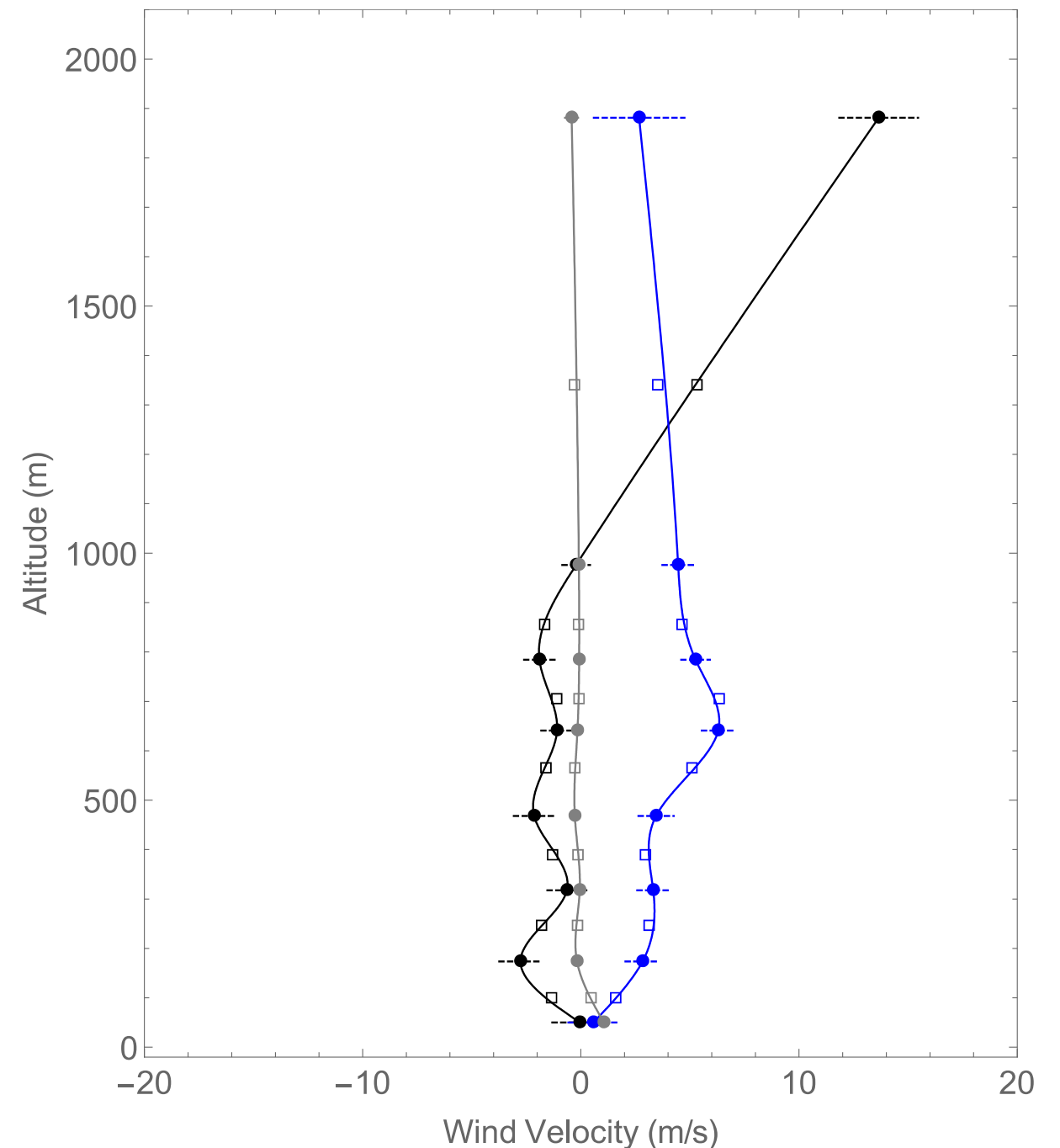
One simply finds the mid points of the spline intervals, ignores the wind velocity variation within an interval and then uses the method of least squares to find the wind vector velocity vector for that interval that best matches the observed Doppler velocities and radar pointing beams.

For each interval this requires computing a solution of the form

$$\mathbf{v}_{LS} = -(\mathbf{B}^T \mathbf{B})^{-1} \mathbf{B}^T \mathbf{V}_{obs}$$

where \mathbf{B} is a matrix whose rows are the radar beam pointing directions for the interval and \mathbf{V}_{obs} are the observed Doppler velocities for the interval arranged in vector format.

Note how closely the method of intervals agrees with the spline solution. This strongly suggests that the spline representation of the wind profile between pivot points makes sense



Check 3) LCRWE spline agrees with velocity inversion by the method of intervals.

Points of Contact

Quinn Smith
QinetiQ Inc.
quinn.smith@us.qinetiq.com
(571)830-7440

Michael Vollmuth
Chief Operating Officer LogLinearGroup
michael.vollmuth@loglineargroup.com
(228)238-1496

Mark Henderson
Chief Engineer LogLinear Group
mark.henderson@loglineargroup.com
(228)697-2221

Marshall Bradley
Chief Scientist LogLinear Group
marshall.bradley@gmail.com
(985)290-4339

Website
<https://loglineargroup.com>